*Cerebral Cortex*, November 2019; 4679–4696

**doi: 10.1093/cercor/bhz002**
Advance Access Publication Date: 31 January 2019
Original Article

ORIGINAL ARTICLE

# Alterations in Oscillatory Behavior of Central Medial Thalamic Neurons Demonstrate a Key Role of $Ca_V3.1$ Isoform of T-Channels During Isoflurane-Induced Anesthesia

Tamara Timic Stamenic [1], Simon Feseha[1], Robert Valdez[2], Wanzhu Zhao[1], Jost Klawitter[1] and Slobodan M. Todorovic[1,3]

[1]Department of Anesthesiology, University of Colorado, Anschutz Medical Campus, Aurora, CO 80045, USA, [2]Department of Pediatrics, Division of Neurology, School of Medicine, Translational Epilepsy Research Program, University of Colorado, Anschutz Medical Campus, Aurora, CO 80045, USA and [3]Neuroscience Graduate Program, University of Colorado, Anschutz Medical Campus, Aurora, CO 80045, USA

Address correspondence to Slobodan M. Todorovic, University of Colorado Anschutz Medical Campus, Department of Anesthesiology, Mail Stop 8130, 12801 E. 17th Avenue, Rm L18-4100, Aurora, CO 80045, USA. Email: slobodan.todorovic@ucdenver.edu

## Abstract

Although the central medial nucleus (CeM) of the thalamus is an essential part of the arousal system for sleep and anesthesia initiation, the precise mechanisms that regulate its activity are not well studied. We examined the role of $Ca_V3.1$ isoform of T-type calcium channels (T-channels) in the excitability and rhythmic activity of CeM neurons during isoflurane (ISO)-induced anesthesia by using mouse genetics and selective pharmacology. Patch-clamp recordings taken from acute brain slices revealed that $Ca_V3.1$ channels in CeM are inhibited by prototypical volatile anesthetic ISO (250 and 500 μM) and selective T-channels blocker 3,5-dichloro-*N*-[1-(2,2-dimethyl-tetrahydro-pyran-4-ylmethyl)-4-fluoro-piperidin-4-ylmethyl]-benzamide (TTA-P2). Both TTA-P2 and ISO attenuated tonic and burst firing modes, and hyperpolarized CeM neurons from wild type (WT) mice. These effects were greatly diminished or abolished in $Ca_V3.1$ null mice. Our ensuing in vivo local field potential (LFP) recordings from CeM indicated that the ability of TTA-P2 and anesthetic concentrations of ISO to promote δ oscillation was substantially weakened in $Ca_V3.1$ null mice. Furthermore, escalating ISO concentrations induced stronger burst-suppression LFP pattern in mutant than in WT mice. Our results demonstrate for the first time the importance of $Ca_V3.1$ channels in thalamocortical oscillations from the non-specific thalamic nuclei that underlie clinically important effects of ISO.

**Key words:** anesthesia, bursting, low-voltage-activated, sedation, sensory processing

## Introduction

T-channels play an important role in synaptic plasticity, cell excitability, and oscillatory behavior (Simms and Zamponi 2014; Leresche and Lambert 2017). T-channels need smaller depolarization for opening and are able to form "window" currents around resting neuronal membrane potential. During hyperpolarization of cells T-channels are deinactivated, so they can open after depolarization and trigger LTS crowned with characteristic rebound burst-firing pattern. There are 3 known isoforms of T-channels, $Ca_V3.1$, $Ca_V3.2$, and $Ca_V3.3$, which are

expressed and localized in different brain regions, including the thalamus (Talley et al., 1999). It has been shown that, in mice lacking $Ca_V3.1$ channels, LTS and burst-firing mode is completely abolished in thalamocortical neurons, whereas the tonic mode firing showed an apparently normal pattern (Kim et al. 2001). In contrast to thalamocortical circuits where the dominant subtype is the $Ca_V3.1$ channel, thalamic reticular nucleus (TRN) – composed from GABAergic neurons and basal forebrain that is involved in the control of wakefulness and cortical rhythms has predominant expression of $Ca_V3.2$ and $Ca_V3.3$ T-channel expression (Talley et al. 1999). Consistent with their important roles in regulation of neuronal excitability, T-channel dysfunction has been implicated in sleep disorder, absence epilepsy, pain, neurological disorders, neuropsychiatric disorders, cognitive disorders, as well as in chronic hyperexcitability of thalamocortical networks following exposure to general anesthesia during brain development (Huc et al. 2009; Miwa and Kondo 2011; Cheong and Shin 2013; Chen et al. 2014; DiGruccio et al. 2015).

The thalamocortical network can generate several types of rhythmic activity under different states of arousal, such as slow oscillations with high amplitudes during sleep and under anesthesia, and distinct faster oscillations during conscious states (Jones 2001). The thalamic intralaminar complex with midline nuclei is a part of non-specific arousing system in the brain (Van Der Werf et al. 2002). It has been shown that high frequency stimulation of non-specific thalamic nuclei can desynchronize the cortex and elicit arousal, while repetitive low frequency stimulation is associated with sleep and drowsiness (Pereira de Vasconcelos and Cassel 2015). The CeM is a part of the rostral intralaminar complex that sends diffuse projections to the anterior and posterior regions of the cortex, the claustrum, the caudate-putamen, the nucleus accumbens, the olfactory tubercle, and the amygdala (Vertes et al. 2012). Although, recent studies revealed that CeM acts as a key hub through which general anesthesia and natural sleep are initiated (Baker et al. 2014; Saalmann 2014; Gent et al. 2018), the role of T-channels in CeM in clinically important effects of general anesthetics is not known.

Previous studies revealed that $Ca_V3.1$ T-channels are inhibited by prototypical volatile anesthetic ISO in the ventro-basal (VB) complex of the thalamus at clinically relevant concentrations (Eckle et al. 2012). Furthermore, mice lacking $Ca_V3.1$ channels exhibit delayed induction with volatile anesthetics including ISO (Petrenko et al. 2007). However, the specific mechanisms of interactions of ISO with ion channels that regulate excitability of CeM neurons and underlying the role of $Ca_V3.1$ channels in thalamocortical oscillations in vivo during general anesthesia with volatile anesthetics are largely unknown. Here, we used patch-clamp recordings from acute brain slices and mouse genetics to investigate mechanisms of ISO inhibition of T-channel dependent excitability of CeM neurons in vitro and LFP recordings in vivo in order to elucidate the role of the $Ca_V3.1$ channels in CeM neurons in thalamocortical oscillations during ISO-induced anesthesia.

## Materials and Methods

### Animals

Experimental procedures with animals were performed according to the guidelines approved by University of Colorado Anschutz Medical Campus. Treatments of mice adhered to guidelines set forth in the NIH *Guide for the Care and Use of Laboratory Animals*. All efforts were made to minimize animal suffering and to use only the number of animals necessary to produce reliable scientific data. Male and female juvenile (young adult) C57BL/6 J (wild type – WT) and $Ca_V3.1$ knockout (KO) mice (postnatal day (P), P25-P35) were used for in vitro electrophysiological recordings while older mice (3 months) were used for in vivo electrophysiological experiments. C57BL/6 J mice were obtained from the Jackson laboratory (USA) while $Ca_V3.1$ KO mice (α1G null) (Ricken BioResources Centre, Japan) were generated on C57BL/6 background as previously described (Petrenko et al. 2007). All animals were maintained on a 12/12 h light-dark cycle with food and water ad libitum.

### In Vitro Brain Slice Preparation

Wild type and $Ca_V3.1$ KO mice of either sex were anesthetized briefly with ISO and decapitated. Their brains were removed rapidly and placed in a cold (4 °C) oxygenated (95 vol% $O_2$ and 5 vol% $CO_2$) solution. Live 250- to 300-μm-thick coronal brain slices were sectioned at 4 °C in the same cold solution (in mM): sucrose 260, D-glucose 10, $NaHCO_3$ 26, $NaH_2PO_4$ 1.25, KCl 3, $CaCl_2$ 2, $MgCl_2$ 2, using a vibrating micro slicer (Laica VT 1200 S). Brain slices were immediately incubated for 30 min in the following solution (in mM): NaCl 124, D-glucose 10, $NaHCO_3$ 26, $NaH_2PO_4$ 1.25, KCl 4, $CaCl_2$ 2, $MgCl_2$ 2 at 37 °C before use in electrophysiology experiments, which were done at room temperature. During incubation, slices were constantly perfused with a gas mixture of 95 vol% $O_2$ and 5 vol% $CO_2$.

### Electrophysiology Experiments

The external solution for voltage and current-clamp electrophysiology experiments consisted of the following (in mM): NaCl 125, D-glucose 25, $NaHCO_3$ 25, $NaH_2PO_4$ 1.25, KCl 2.5, $MgCl_2$ 1, $CaCl_2$ 2. For voltage-clamp experiments, tetrodotoxin (TTX; 1 μM) was added to the extracellular medium as a voltage-dependent sodium current blocker, while current-clamp experiments contained the synaptic blockers picrotoxin (20 μM), D-2-amino-5-phosphonovalerate (D-AP5; 50 μM), and 2,3-dihydroxy-6-nitro-7-sulfamoyl-benzo[f]quinoxaline-2,3-dione (NBQX; 5 μM) in the extracellular medium. For current-clamp experiments, the internal solution consisted of the following (in mM): potassium-D-gluconate 130, ethylene-glicol-bis(β-aminoethylether)*N*,*N*,*N*′,*N*′-tetraacetic acid (EGTA) 5, NaCl 4, $CaCl_2$ 0.5, HEPES 10, Mg ATP 2, Tris GTP 0.5, pH 7.2.

The internal solution for voltage-clamp experiments with cesium (Cs) consisted of the following (in mM): Cs-methanesulfonate 110, phosphocreatine 14, HEPES 10, EGTA 9, Mg-ATP 5, and Tris-GTP 0.3, pH adjusted to 7.15–7.20 with CsOH (standard osmolarity: 300 mOsm) (Stamenic and Todorovic 2018).

Whole-cell recordings were performed in CeM neurons visualized under Zeiss optics (Zeiss AXIO Examiner D1, 40× objective). Glass microelectrodes (Sutter Instruments, borosilicate glass with filament OD 1.2 mm) were pulled using a Sutter Instruments P-1000 model and fabricated to maintain an initial resistance of 3–6 MΩ. Neuronal membrane responses were recorded using a Multiclamp 700 B amplifier (Molecular Devices, Foster City, CA, USA). Voltage current commands and digitization of the resulting voltages and currents were performed with Clampex 8.3 software (Molecular Devices) running on a PC-compatible computer. Resulting current and voltage traces were analyzed using Clampfit 10.5 (Molecular Devices). Statistical and graphical analyses were performed using

GraphPad Prism 7.0 software (GraphPad Software) or Origin 7.0 (OriginLab). Results typically are presented as means ± SEM unless stated otherwise.

### Voltage-Clamp Experiments

T-channel activation was measured by stepping the membrane potential from an initial holding potential ($V_h$) of −90 mV to test potentials ($V_t$) from −80 to −40 mV in 2.5 mV increments over a period of 320 ms. Current–voltage (*I–V*) curves were generated, and peak current amplitudes and inactivation properties of current waveforms were established. We calculated current densities by measuring average peak current divided by the capacitance of the neuron. Steady-state inactivation curves were generated by using a standard double-pulse protocol with 3.6-s-long prepulses to variable voltages (from −120 to −60 mV in 5 mV increments) and test potentials to −50 mV. The voltage dependencies of activation and steady-state inactivation were described with single Boltzmann distributions of the following forms:

$$\text{Activation: } G(V) = G_{max}/(1 + \exp[-(V - V_{50})/k])$$

$$\text{Inactivation: } I(V) = I_{max}/(1 + \exp[(V - V_{50})/k])$$

In these forms, $I_{max}$ is the maximal amplitude of current, $G_{max}$ is the maximal conductance (calculated by dividing current amplitude by estimated reversal potential), $V_{50}$ is the voltage at which half of the current is activated or inactivated, and $k$ represents the voltage dependence (slope) of the distribution.

Additionally, in experiments with the pharmacological blocker TTA-P2 or ISO, T-current was elicited by stepping to −50 mV from a holding potential of −90 mV every 20 s 5 times.

### Methodological Considerations for Slice Recordings

Recordings from intact brain slices offer great advantages for studying neurons in an intact setting in vitro. However, the presence of extensive processes may compromise voltage control so that all biophysical measurements must be interpreted with caution. Accordingly, we paid close attention to the signs of good voltage control. Specifically, there was no extensive delay in the onset of current; also, the onset and offset kinetics depended on voltage, not on the amplitude of current. In whole-cell experiments, because intact thalamic neurons have long processes, rapid components of recorded current, such as tail current, are unlikely to reflect the true amplitude and time course of calcium current behavior. For the same reasons, we did not attempt to quantify macroscopic current activation kinetics in CeM neurons. All of our measurements of amplitudes from holding, peak, and steady-state currents were made at time points sufficient to ensure reasonably well-clamped current condition. In addition, delivery of drug-containing solutions in vitro may be compromised due to diffusion through the slice tissue. Therefore, the actual concentrations of all compounds at their sites of action are likely to be lower than those reported.

### Current-Clamp Experiments

Both tonic and burst-firing properties of CeM neurons were characterized by using multistep protocols in WT and $Ca_V3.1$ KO mice. To investigate tonic firing patterns in CeM cells, we injected a depolarizing current pulse through the recording pipette of 400 ms duration in 25 pA incremental steps starting from 50 pA. To investigate burst-firing patterns, the neurons were injected with hyperpolarizing currents in 25 pA intervals stepping from 0 to −225 pA. Subsequent resting membrane potentials (RMP), tonic action potential (AP) frequencies, LTS amplitude, threshold to LTS and input resistances (IR) were determined. RMP was measured at the beginning of each recording and was not corrected for the liquid junction potential.

### LFP Data Acquisition and Spectral Analysis

Synchronized, time locked video and LFP signals were recorded using the Pinnacle system (Pinnacle Technology Inc., Lawrence, KS, USA). The LFP signals were amplified (100×) and digitized at a sampling frequency rate of 2000 Hz (high pass filter 0.5 Hz and low pass filter 500 Hz) and stored on a hard disk for offline analysis. The electrodes (one depth coated tungsten in CeM [anteroposterior – AP: −1.35 mm, mediolateral – MD: 0 and dorsoventral – DV: −3.6 mm], and two screw-type cortical [AP: −1 mm, MD: ± 3 mm, DV: 0]) were implemented under continuous 2.5 vol% ISO anesthesia. Banamine® – Merck (intraperitoneal (i.p.) 2.5 mg/kg) was applied right after surgery and every 24 h for 48 h. Seven to ten days after surgery WT and $Ca_V3.1$ KO mice of both sex (7 WT and 10 KO) were put in recording chamber ((H × W × L) 15.2 × 16.5 × 31.1 cm) and LFPs were recorded 15 min before i.p. administration of 2-hydroxypropyl-β-cyclodextrin (15%) – baseline recordings. Anesthesia with ISO was initiated 15 min after 2-hydroxypropyl-β-cyclodextrin administration, starting from 1 to 2 vol% of ISO (increasing 0.2 vol% of ISO every 5 min) and LFPs were recorded the whole time under ISO.

To compare spectra, 4 min of signal in baseline and during 1 or 2 vol% of ISO were extracted. LFPs from the cortex were not analyzed for this study. The suppression-to-burst (BSR) ratio was calculated by dividing suppression time with total time under one concentration of ISO.

For experiments with the pharmacological blocker TTA-P2, in vivo baseline was recorded for 15 min. After injection of TTA-P2 (i.p. 60 mg/kg) the LFPs were recorded for 45 min. To compare spectra, 5 min of baseline and after TTA-P2 injection (30 min after application) were extracted. All spectral analysis was carried out using the LabChart 8 and Origin 2018 software. The relative (%) power is calculated for different frequency range: δ (0.5–4 Hz), θ (4–8 Hz), α (8–13 Hz), β (13–30 Hz) and low γ (30–50 Hz). Additionally, power density ($\mu V^2$/Hz) and spectrogram for whole frequency range (0.5–50 Hz) were analyzed.

After completion of experiments, mice were anesthetized with ketamine (100 mg/kg i.p.) and electrolytic lesions were made by passing 5 μA current for 1 s (5 times). Mice were anesthetized additionally with ISO and perfused with ice-cold 0.1 M phosphate buffer containing 1% of potassium-ferrocyanide. The brains were extracted, kept in 4% formalin (PFA) for 2 days and sliced (100–150 μm) using a vibrating micro slicer (Laica VT 1200 S). Photos of coronal slices with electrode location conformation were obtained using bright-field Zeiss stereoscope and Zen Blue software.

### Drugs

TTX, TTA-P2, and SNX-482 were purchased from Alomone Lab (Jerusalem, Israel). Sevoflurane and ISO were purchased from McKesson (San Francisco, CA), 2-hydroxypropyl-β-cyclodextrin solution from Santa Cruz Biotechnology (Dallas, TX), ketamine and Banamine® (Merck) were obtained from the pharmacy. All

other compounds were purchased from Sigma Chemical (St. Louis, MO). Pan-selective T-type calcium channel blocker TTA-P2 was prepared as a 5 mM stock solution in dimethylsulfoxide (DMSO) for electrophysiological experiments; aliquots were stored at −20 °C and diluted for use at a final concentration of 5 μM which was delivered with a gravity-driven perfusion system. Selective R-type calcium channel blocker SNX-482 was prepared as a 0.5 mM stock solution in DMSO for electrophysiological experiments; aliquots were stored at −20 °C and diluted for use at a final concentration of 0.5 μM which was delivered with a gravity-driven perfusion system. For LFP recordings, TTA-P2 was dissolved/suspended in 15% of 2-hydroxypropyl-β-cyclodextrin solution and injected i.p. (60 mg/kg). Aliquots of ISO were prepared from saturated external solution incubated with ISO (30 mL of external with 20 mL of ISO in a closed 50 mL vial) for at least 24 h at −4 °C as described in Joksovic and Todorovic (2010). To quantify the actual ISO concentrations in solutions, we analyzed 1/10 diluted samples of the original saturated stock solutions (mean ± SD = 6.96 ± 0.50 mM, 2 samples) using a headspace gas chromatography mass spectrometry (HS-GC/MS) based assay calibrated with the appropriate anesthetic standards in the range between 0.11 and 2.775 mM. Samples were diluted and analyzed in triplicate to confirm the accurate concentrations. We used a modification of the method described by Accorsi et al. (2003) for the ISO analysis. Sevoflurane was used as an internal standard. An Agilent GC-MS system (5973 Network Mass Selective detector and 6890 N GC system, Agilent Technologies, Palo Alto, CA) connected to a Tekmar 7000 headspace autosampler (Teledyne Tekmar, Mason, OH) was used as HS-GC/MS system. The masses of *m*/*z* 51, 67, and 149 were used for ISO quantitation. Aliquots (test solutions) for concentration–response curves were prepared from external solution containing ISO in closed syringe by diluting stock solution in order to get different ISO concentration.

### Data Analysis

In every in vitro experiment, we attempted to obtain as many neurons as possible from each animal to minimize the number of animals used. Statistical analysis was performed using two-way repeated measure (RM) ANOVA (in TTA-P2 and ISO electrophysiology experiments both factors were repeated), as well as Student unpaired and paired two-tailed *t*-test where appropriate. Where interaction between factors after two-way RM ANOVA was significant, Sidak's post hoc comparisons were used. Significance was accepted with *P* values <0.05. Statistical and graphical analysis was performed using GraphPad Prism 7.00 software (GraphPad Software, La Jolla, CA, USA) and Origin 2018 (OriginLab, Northampton, MA, USA). LFPs were analyzed using LabChart 8 (ADInstruments, Dunedin, New Zealand).

## Results

### Biophysical Properties of T-Currents in Wild Type and $Ca_V3.1$ KO Mice

In order to examine the biophysical properties of isolated T-channels in the CeM in WT and $Ca_V3.1$ KO mice we used a Cs-containing internal solution (Stamenic and Todorovic 2018). The representative traces from a current–voltage (*I*–*V*) experiment showing properties of voltage-dependent activation of T-currents from WT mice (black) and inward currents from $Ca_V3.1$ KO mice (gray) are presented in Figure 1*A*. Note that T-currents from WT mouse show characteristic crisscrossing pattern that was not observed in traces of inward currents from $Ca_V3.1$ KO mouse. In addition, traces from the mutant mice show drastically slower macroscopic current kinetics when compared with the WT mice. Representative traces from voltage-dependent inactivation of T-currents of CeM neurons over a wide range of prepulse potentials are presented in Figure 1*B* (black – WT and gray – $Ca_V3.1$ KO mice). The average $V_{50}$ value for T-current activation for $Ca_V3.1$ KO mice was at much more depolarized voltage than in WT mice (Fig. 1*C*). The difference between $V_{50}$ for T-current activation (for about 20 mV) was statistically significant between WT and mutant mice. On the contrary, the difference between $V_{50}$ for T-current inactivation was not statistically significant between WT and mutant mice (Fig. 1*D*). The maximal current density for T-current activation from WT mice (Fig. 1*E*) and inactivation (data not shown) was more than 10-fold bigger than the maximal current density recorded from $Ca_V3.1$ KO mice. The Sidak's post hoc tests for difference in T-current density for steady-state activation between WT and mutant mice are presented in Figures 1*E*. Note that the time constant of macroscopic T-current inactivation (Fig. 1*F*) recorded from WT mice was about 4.5-fold faster than the time constant for the currents obtained from $Ca_V3.1$ KO mice. Additionally, there is a noticeable window current in WT mice obtained by overlapping $I/I_{max}$ and $G/G_{max}$ curves (black), which is absent in $Ca_V3.1$ KO mice (gray) due to the observed depolarizing shift of activation curves (Fig. 1*G*). This very slow inactivation time constant, 20 mV depolarizing shift in activation curves and absence of crisscrossing pattern in our current–voltage relationships strongly suggests a lack of canonical T-currents in CeM neurons from $Ca_V3.1$ KO mice. This is in accordance with previous studies that have shown using in situ hybridization that the main isoform of T-channels in the CeM is $Ca_V3.1$ (Talley et al. 1999).

Virtually all of the CeM neurons from WT mice in our study displayed inward currents with typical properties of T-currents as we observed in rats (Stamenic and Todorovic 2018). In contrast, recordings from $Ca_V3.1$ KO mice revealed that only 36.8% of cells (total 38 cells) had small inward currents that have characteristics resembling high-voltage-activated (HVA) calcium currents. Next, we set out to interrogate remaining inward currents in CeM neurons from the mutant mice. We recorded our standard *I*–*V* protocols before and after applications of 0.5 μM SNX-482, a selective $Ca_V2.3$ R-type calcium channel blocker (Fig. 1*H*). We found that peak current amplitudes in the mutant mice were reduced in average for about 30% in the range of test potentials from −50 to −42.5 mV in the presence of SNX-482 when compared with the baseline currents in the same neurons. This strongly suggests that inward currents with slower kinetics in CeM neurons from the mutant mice are, at least in part, arising from the $Ca_V2.3$ subtype of HVA calcium channels.

### Excitability of CeM Neurons in Wild Type and $Ca_V3.1$ KO Mice

It has been known that CeM neurons, as well as cells from other thalamic nuclei, may fire action potentials (APs) in both tonic and post-inhibitory rebound burst firing modes (Jhangiani-Jashanmal et al. 2016; Stamenic and Todorovic 2018). The ability of T-channels to recover from inactivation during hyperpolarization makes them critical contributors to burst firing mode. In addition, at more depolarized membrane potentials, when most of the T-channels are inactivated, the tonic-firing mode is predominant. To investigate the contribution of $Ca_V3.1$

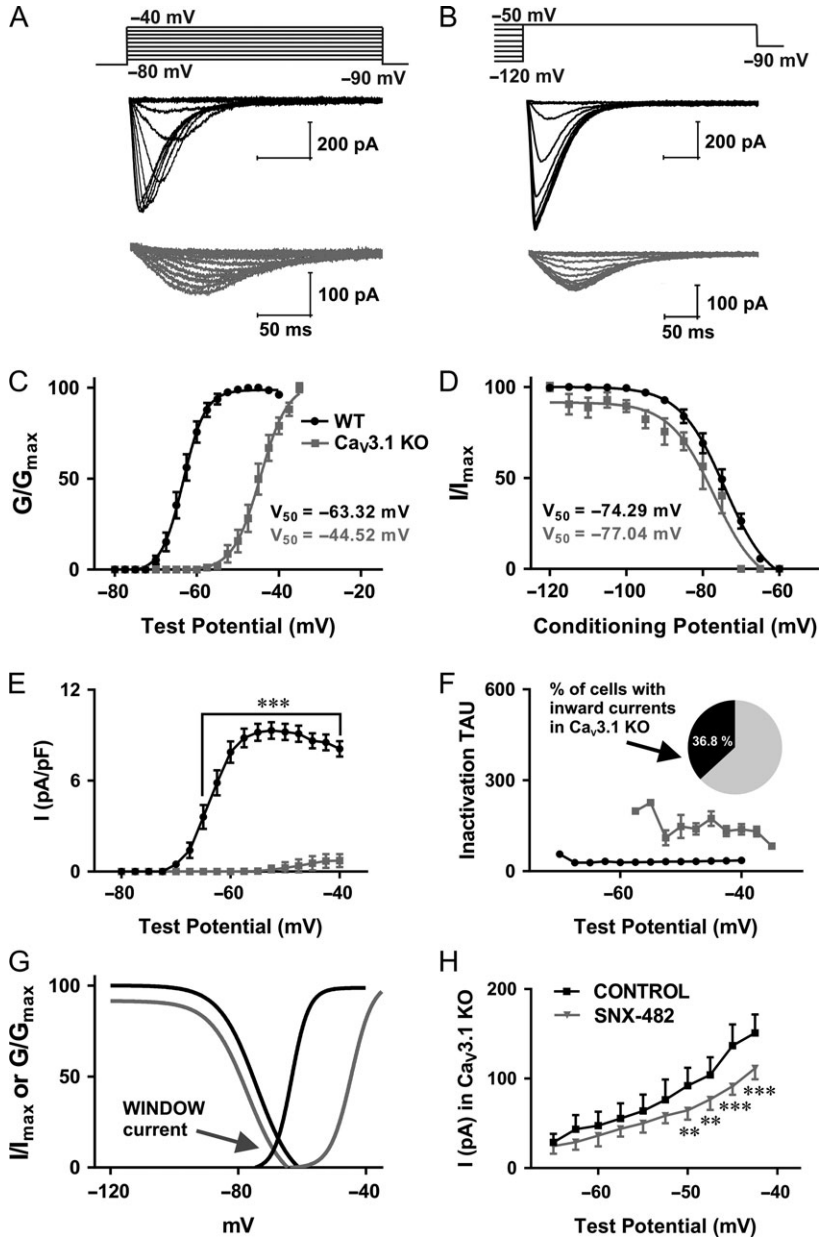


**Figure 1.** Biophysical properties of CeM T-currents in WT and $Ca_V3.1$ KO mice. *A*, T-current *I–V* traces from representative CeM neurons in the voltage range for $V_t$ of –80 to –40 mV from an initial holding potential ($V_h$) of –90 mV in 2.5 mV increments recorded from WT (black) and $Ca_V3.1$ KO mice (gray). *B*, T-current traces from representative CeM neurons showing voltage-dependent inactivation of T-currents from WT mice (black) and inward currents from $Ca_V3.1$ KO mice (gray) generated using a double-pulse protocol with 3.6-s-long prepulses to variable voltages (from –120 to –50 mV in 5 mV increments) and a test potential ($V_t$) of –50 mV. *C*, the average voltage dependence of a steady-state activation ($G/G_{max}$) curve with $V_{50}$ value noted on the graph for WT and $Ca_V3.1$ KO mice. The difference between $V_{50}$ for T-current activation was statistically significant between WT and mutant mice: unpaired two-tailed *t*-test $t_{(40)} = 34.24$, $P < 0.001$. The average $V_{50}$ value for T-current activation for WT mice was –63.3 ± 0.3 mV (28 cells, 3 animals) with respective slope factors of 2.7 ± 0.2 (black). The average $V_{50}$ value for inward current activation for $Ca_V3.1$ KO mice was –44.5 ± 0.5 mV (14 cells had currents from total of 38 patched cells, 4 animals) with respective slope factors of 3.3 ± 0.4 (gray). *D*, the average steady-state inactivation ($I/I_{max}$) curves with $V_{50}$ values are noted on the graph. The difference between $V_{50}$ for T-current inactivation was not statistically significant between WT and mutant mice: unpaired two-tailed *t*-test $t_{(24)} = 1.64$, $P = 0.11$. For experiments with WT mice, the average $V_{50}$ value for steady-state inactivation was –74.3 ± 0.8 mV (20 cells, 3 animals) with a slope factor of 5.9 ± 0.6 mV (black). The average $V_{50}$ value for steady-state inactivation from $Ca_V3.1$ KO mice was –77.0 ± 1.5 mV (6 cells had inward currents from total 38 recorded cells (15.9%), 3 animals) with a slope factor of 5.9 ± 1.3 mV (gray). *E*, average current density from multiple *I–V* curves; two-way RM ANOVA: interaction $F_{(15,00)} = 48.05$, $P < 0.001$; voltage $F_{(15,00)} = 54.14$, $P < 0.001$; WT vs. mutant $F_{(1,40)} = 112.30$, $P < 0.001$, Sidak's post hoc presented in figure. The maximal current density for current activation from WT mice was 9.31 pA/pF at –52.5 mV, while the maximal current density for current activation recorded from $Ca_V3.1$ KO mice was only 0.73 pA/pF at –40 mV. *F*, inactivation tau values for I–V T-currents from WT mice and inward currents recorded in 36.8% of all patched CeM cells (38 cells in total) from $Ca_V3.1$ KO mice. The time constant of macroscopic T-current inactivation (Vt = –52.5 mV, 31.46 ms) recorded from WT mice was about 4.5-fold faster than time constant obtained from $Ca_V3.1$ KO mice (Vt = –40 mV, 138.42 ms). *G*, the lack of window current in $Ca_V3.1$ KO mice. *H*, average current amplitude, as calculated from the steady-state activation protocol before and after application of SNX-482 in $Ca_V3.1$ KO mice (4 cells, two-way RM ANOVA: interaction $F_{(9,27)} = 4.70$, $P < 0.001$; voltage $F_{(9,27)} = 58.37$, $P < 0.001$; SNX-482 $F_{(1,3)} = 5.43$, $P = 0.102$, Sidak's post hoc presented in figure). The average maximal current amplitude for steady-state activation in $Ca_V3.1$ KO animals was 150.90 pA (black) at –42.5 mV, while after SNX-482 perfusion average maximal current amplitude was 111.40 pA (gray). $^{**}P < 0.01$, $^{***}P < 0.001$.

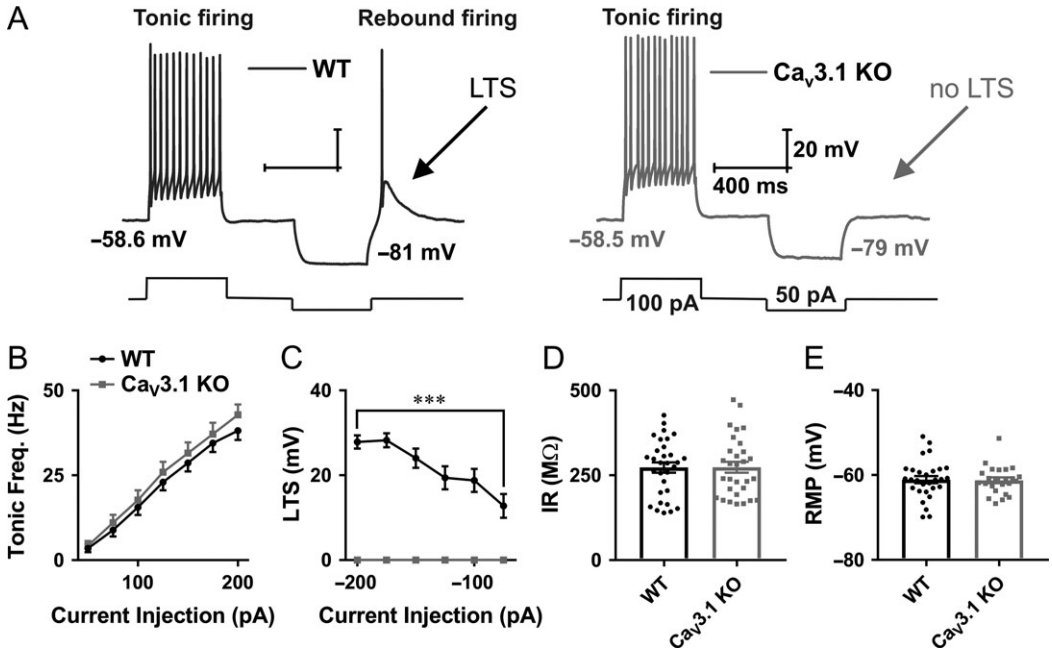


**Figure 2.** Different patterns of excitability of CeM neurons in WT and $Ca_V3.1$ KO mice. *A*, Original traces from representative neurons in the CeM recorded from WT (left panel, black trace) and $Ca_V3.1$ KO mice (right panel, gray trace) show active membrane responses to a depolarizing (100 pA) and hyperpolarizing (−50 pA) current injection. Note that CeM neuron from $Ca_V3.1$ KO mice does not show APs with low threshold spike (LTS) after membrane hyperpolarization. *B*, Graph of averages of tonic AP firing frequency and current injections of 50–200 pA from multiple experiments shows no difference between WT and mutant mice (WT – 31 cell, 10 animals, $Ca_V3.1$ KO – 30 cells, 9 animals; two-way RM ANOVA: interaction $F_{(6354)} = 0.45$, $P = 0.85$; current injection $F_{(6354)} = 244.00$, $P < 0.001$; WT vs. mutant $F_{(1,59)} = 0.63$, $P = 0.43$). *C*, Graph of averages of LTS amplitudes from multiple experiments following escalating current injections ranging from −50 to −200 pA (WT – 31 cell, $Ca_V3.1$ KO. – 28 cells). Recordings from $Ca_V3.1$ KO mice (gray line) show no LTS as a response to hyperpolarizing current injections (two-way RM ANOVA: interaction $F_{(5285)} = 16.51$, $P < 0.001$, current injection $F_{(5258)} = 16.51$, $P < 0.001$ and WT vs. mutant $F_{(1,57)} = 110.9$, $P < 0.001$, Sidak's post hoc presented in figure). *D*, IR recorded with 75 pA hyperpolarizing current injection, WT – 31 cells, $Ca_V3.1$ KO – 30 cells; unpaired two-tailed *t*-test: $t_{(59)} = 0.04$, $P = 0.97$. *E*, average RMP, WT – 29 cells, $Ca_V3.1$ KO – 14 cells; unpaired two-tailed *t*-test: $t_{(51)} = 0.15$, $P = 0.88$. ***$P < 0.001$.

T-channels on excitability of CeM neurons, we recorded firing patterns of APs in WT and $Ca_V3.1$ KO mice. Representative traces from WT (black trace) and $Ca_V3.1$ KO (gray trace) mice are presented in Figure 2A. The tonic frequency recorded from CeM cells was apparently not altered in $Ca_V3.1$ KO in comparison to WT mice (WT – black, $Ca_V3.1$ KO – gray, Fig. 2B). In contrast, while all CeM WT neurons exhibit a characteristic LTS and burst-firing mode after periods of membrane hyperpolarization, CeM neurons from $Ca_V3.1$ KO mice did not show any APs nor LTS after membrane hyperpolarization. The average LTS amplitude from two mouse cohorts is presented in Figure 2C. Additionally, we found that IR recorded with 75 pA hyperpolarizing current injection (Fig. 2D) and average RMP were not different between WT and $Ca_V3.1$ KO mice (Fig. 2E).

## Voltage-Dependent Inhibition of T-Currents in CeM Neurons at Clinically Relevant Concentration of ISO

We next examined the effects of ISO on T-current densities and kinetics in CeM. Representative traces from recordings designed to study effects of ISO on voltage-dependent T-current inactivation are presented in Figure 3A (black traces – baseline from WT mice; gray traces – after 5–10 min of ISO perfusion). The concentration–response curves for ISO inhibition of T-currents in WT CeM neurons under two recording voltages (−70 mV and −90 mV) are presented in Figure 3B. Note that $IC_{50}$ value for current inhibition by ISO at $V_h$ of −70 mV was about 330 μM and at −90 mV it was about 463 μM, indicating higher potency of channel block at more depolarized membrane potentials. The clinically relevant concentration of ISO for the experiments conducted at room temperature in vitro in most species was estimated to be between 120 and 600 μM, which is equivalent to roughly 0.5–2.5 vol% inhaled concentrations in vivo (Mandal and Pettegrew 2008). Additionally, the minimal alveolar concentration (1 MAC) for ISO in C57BL/6 mice is equivalent to 1.3 vol% (Sonner et al. 1999), while 1.3 vol% is equivalent to 310 μM of ISO (Sonner et al. 2007). Therefore, we used a 500 μM ISO concentration for subsequent in vitro experiments that would be equivalent to very high concentration used for in vivo LFP recordings (Franks and Lieb 1993). Figure 3C shows plots the average steady-state inactivation curves and average $V_{50}$ values for baseline (black curve) and ISO (gray curve). The hyperpolarizing shift in steady-state inactivation of about 9 mV recorded after ISO perfusion was statistically significant when compared with the control conditions. Similarly, ISO perfusion significantly decreased current density by 40–80% over the wide range of conditioning potentials (Fig. 3D). Representative average traces of T-current activation before and after perfusion with ISO are shown in Figure 3E (black – baseline; gray trace – same cell with ISO, light gray – wash). Plots in Figure 3F,G show that ISO reduced T-current density by 54% and decreased inactivation tau by about 40% (from 35.20 ms to 20.85 ms).

## Inhibition of T-Currents in CeM Neurons by TTA-P2

Previous studies have established that TTA-P2 exerts a specific and potent inhibition ($IC_{50}$ from 0.02 to 0.1 μM) of native and recombinant T-currents, with minimal effect on native HVA

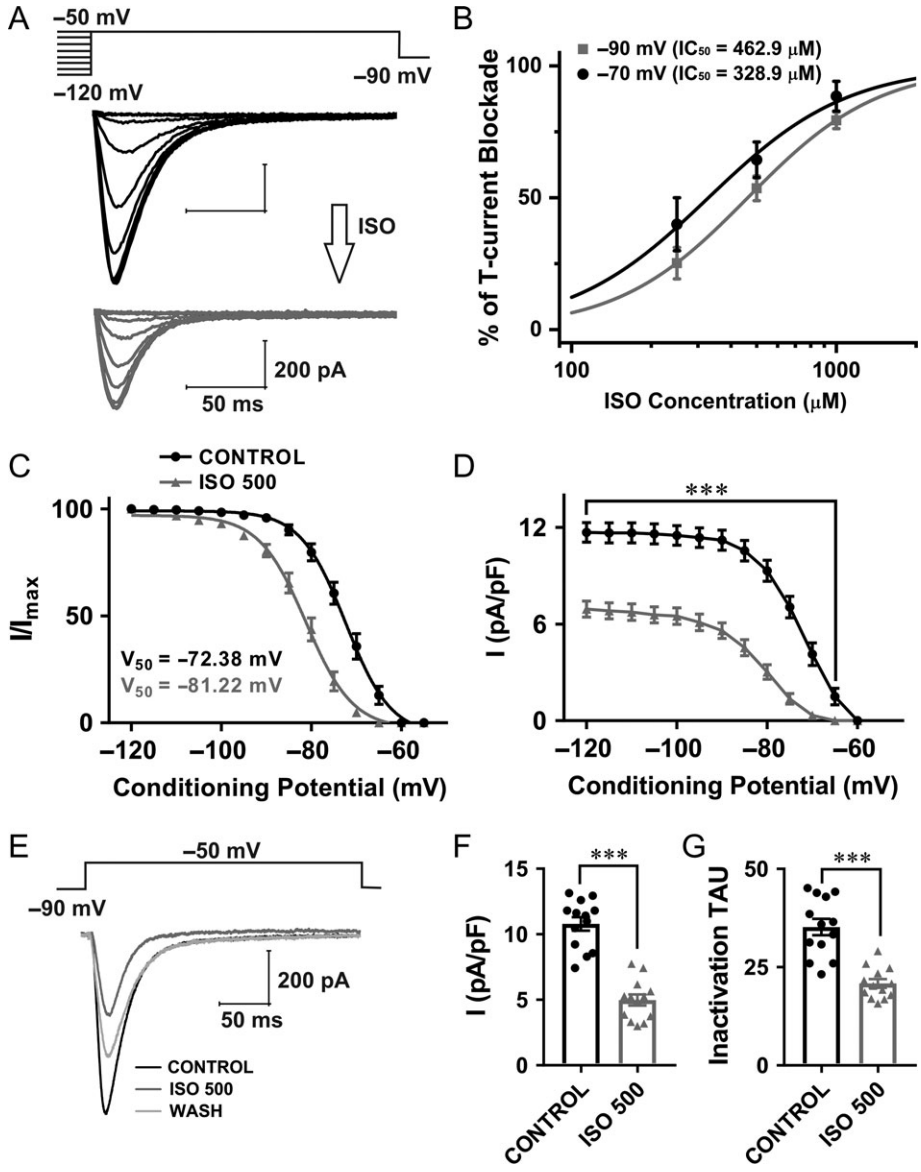


**Figure 3.** Voltage-dependent inhibition of T-currents in CeM WT neurons by clinically relevant concentration of ISO. *A*, T-current traces from a representative CeM neuron generated using a double-pulse protocol with 3.6-s-long prepulses for variable voltages (from –120 to –50 mV in 5 mV increments) and a test potential ($V_t$) of –50 mV; black traces recorded before and gray trace after ISO perfusion. *B*, The concentration–response curves for ISO inhibition of T-currents in WT CeM neurons under two recording voltages (–70 mV and –90 mV) with respective $IC_{50}$ values. *C*, Normalized average steady-state inactivation ($I/I_{max}$) curve, depolarizing shift of 8.8 mV in a cohort of neurons after ISO perfusion was statistically significant from a control cohort (paired two-tailed *t*-test: $t_{(24)} = 12.96$, $P < 0.001$). The average $V_{50}$ values for steady-state inactivation for baseline was –72.4 ± 0.5 mV (black curve; 13 cells, 6 animals) and for ISO –81.2 ± 0.4 mV (gray curve). Slope factors for control and ISO were similar (5.0 ± 0.4 and 5.2 ± 0.4, respectively). *D*, Average current density, as calculated from the steady-state inactivation protocol. Perfusion with ISO significantly decreased current density by approximately 2-fold (two-way RM ANOVA: interaction $F_{(12,144)} = 26.95$, $P < 0.001$; voltage $F_{(12,144)} = 165.00$, $P < 0.001$; ISO $F_{(1,12)} = 122.90$, $P = 0.43$, Sidak's multiple comparison presented in figure). *E*, Averaged representative traces recorded under control conditions (black), after application of ISO (gray) and after wash (light gray trace) using a protocol depicted on the top of traces ($V_t = –50$ mV, $V_h = –90$ mV). *F*, Averaged current density show reduction in current density by 54% after application of ISO (13 cells, 6 animals; paired two-tailed *t*-test: $t_{(12)} = 9.38$, $P < 0.001$). *G*, ISO decreased averaged inactivation tau from 35.20 ms (control conditions) to 20.85 ms (13 cells, 6 animals; paired two-tailed *t*-test: $t_{(12)} = 7.58$, $P < 0.001$). ***$P < 0.001$.

calcium currents, voltage-gated sodium currents, as well as recombinant L-type and R-type HVA currents at concentrations up to 10 μM (Shipe et al. 2008; Dreyfus et al. 2010; Choe et al. 2011). Hence, we used low micromolar concentrations of TTA-P2 (5 μM) in order to exclude any possible off-target effects. Representative current traces of a steady-state inactivation protocol recorded from WT mice are presented in Figure 4A. The upper panel shows traces of T-currents of a CeM neuron under control conditions (black trace) and the lower panel shows traces from the same cell 5 min after perfusion with 5 μM TTA-P2 (gray trace). Perfusion with TTA-P2 resulted in a significant hyperpolarizing shift of about 12 mV in steady-state inactivation $V_{50}$ (Fig. 4B). Representative average traces of T-current activation with a single depolarizing step protocol before and after perfusion with TTA-P2 are depicted in Figure 4C (black – baseline current; gray trace – current in same cell with TTA-P2). Plots in Figure 4D show that TTA-P2 reduced T-current density by 85%, but it did not change inactivation tau (Fig. 4E). The small amplitude of remaining inward current likely represents a fraction of the total T-current that was not blocked by 5 μM

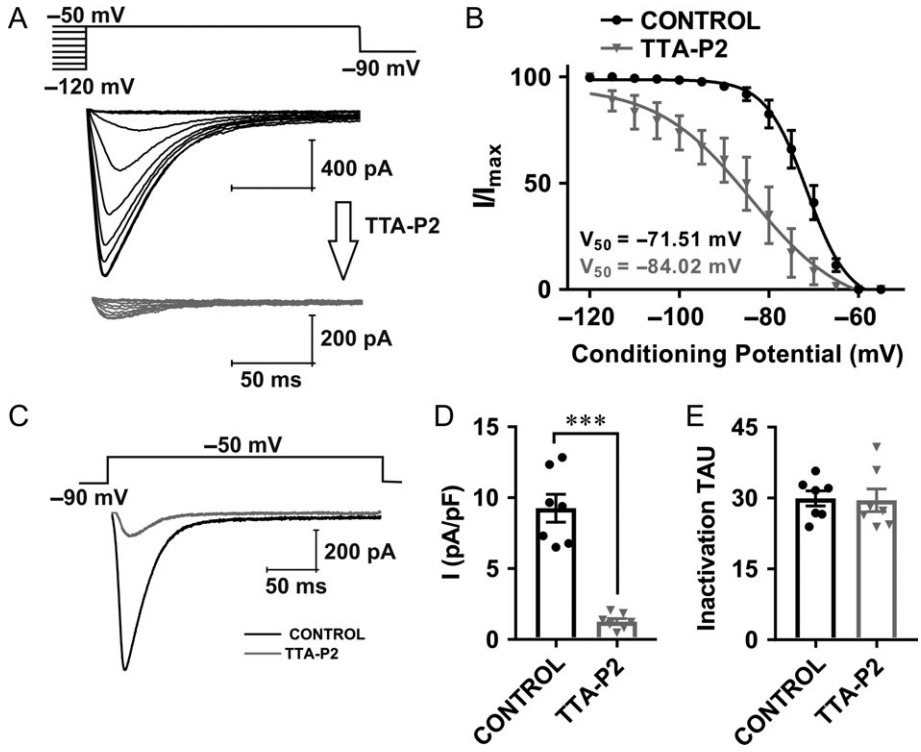


**Figure 4.** Voltage-dependent T-current inhibition by TTA-P2 in CeM neurons from WT mice. A, Traces of T-current in a representative CeM neuron in control conditions (WT mice) recorded using a double-pulse protocol with 3.6-s-long prepulses to variable voltages (from −120 to −50 mV in 5 mV increment, black); traces from the same cell using the identical voltage-protocol during an apparent steady-state inhibition of T-current in the presence of 5 μM TTA-P2 (gray). B, Average normalized steady-state inactivation ($I/I_{max}$) curves in control conditions and after application of TTA-P2 in the same cells with respective $V_{50}$ values. TTA-P2 induced a hyperpolarizing shift in $V_{50}$ of 12.5 mV (two tailed unpaired *t*-test: $t_{(12)} = 4.16$, $P = 0.001$). The average $V_{50}$ value for steady-state inactivation was −71.5 ± 0.7 mV with slope factor of 4.6 ± 0.6 in control conditions (black, 7 cells, 3 animals). After TTA-P2 perfusion of the same cells, the $V_{50}$ value was −84.0 ± 2.9 mV with slope factor of 10.4 ± 3.3 (gray). The slope factor was not significantly different after TTA-P2 perfusion (unpaired two-tailed t-test, $t_{(12)} = 1.75$, $P = 0.106$). C, Averaged representative traces recorded under control conditions (black) and after application of TTA-P2 (gray) using a protocol depicted on the top of traces ($V_t$ = −50 mV, $V_h$ = −90 mV). D, Averaged normalized current density ($V_t$ = −50 mV, $V_h$ = −90 mV) show reduction in current density by 85.36 ± 9.09% (mean ± SD) after application of TTA-P2 (7 cells, 3 animals; two-tailed paired *t*-test: $t_{(6)} = 8.44$, $P < 0.001$). E, TTA-P2 did not significantly affect inactivation tau (7 cells, 3 animals; two-tailed paired *t*-test: $t_{(6)} = 0.14$, $P = 0.89$). ***$P < 0.001$.

TTA-P2, since HVA calcium currents have typically several-fold slower inactivation time constant (Perez-Reyes 2003).

## ISO Diminished both Tonic and Burst Firing of CeM Neurons by Inhibiting $Ca_V3.1$ Channels

In order to examine the consequences of T-current inhibition with ISO on intrinsic excitability of CeM neurons, we monitored their firing patterns of APs using current-clamp recordings. In these experiments, we injected a series of depolarizing and hyperpolarizing currents of the same duration in order to assess tonic firing, membrane IR, and to quantify rebound burst firing. We first noticed that perfusion with ISO reversibly inhibited the number of APs evoked by depolarizing current injections of 100 pA (Fig. 5A). Tonic firing frequency recorded at −60 mV across all current pulses from 50 to 200 pA was decreased by approximately 50% after slices were perfused with ISO in WT animals (Fig. 5B). Interestingly, we found that RMP was significantly hyperpolarized after ISO perfusion for about 7 mV (Fig. 5C), while IR was not significantly changed (Fig. 5D) in WT mice. When injection of hyperpolarizing current was sufficient to remove inactivation of T-currents, neurons showed rebound LTS and burst-firing mode in the control conditions. Traces from a representative neuron with a hyperpolarizing current injection of 150 pA before application of ISO (black trace), after application of ISO (gray trace) and wash (light gray trace) in WT mice are shown in Figure 5E. The average inhibitory effect of ISO on the LTS amplitude from multiple CeM neurons over the range of escalating current injections is presented in Figure 5F. Furthermore, the neuronal cell membrane needed to be significantly more hyperpolarized in order to reach the threshold for LTS after ISO perfusion (Fig. 5G).

In contrast to WT mice, ISO had a minimally inhibitory effect on tonic firing frequency in $Ca_V3.1$ KO mice that was significant only at the most depolarized current injections (Fig. 5H). In addition, we found that ISO did not significantly affect RMP or IR in $Ca_V3.1$ KO mice (Fig. 5I,J). The inhibitory effect of ISO on tonic firing that we observed in the mutant mice could be due to the reported effects of volatile general anesthetics (e.g., sevoflurane) on voltage-gated potassium channels in CeM neurons (Lioudyno et al. 2013), or alternatively other ionic conductances sensitive to ISO.

## Pharmacological Inhibition of T-Currents with TTA-P2 also Reduces Tonic and Rebound Burst Firing in CeM Neurons from WT Mice

Next, we set of to determine whether selective blockers of T-channel like TTA-P2 may mimic the effects of ISO on excitability of CeM neurons in WT mice. It has been demonstrated that high-

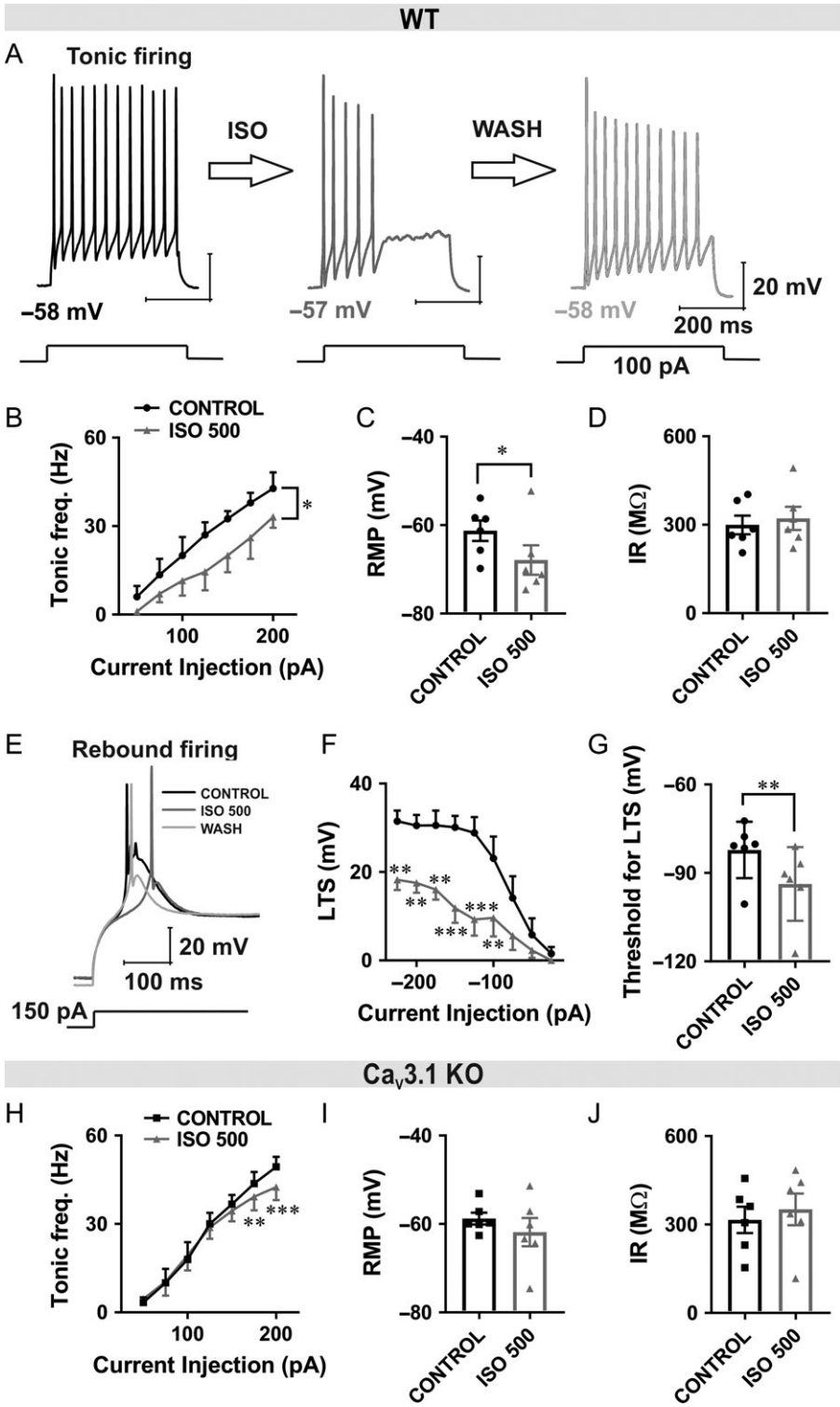


**Figure 5.** Diminished inhibitory effect of ISO on excitability of CeM neurons from $Ca_V3.1$ KO mice. *A*, Original traces from a representative WT neuron in the CeM before application of ISO (black), after application of ISO (gray) and after wash (light gray trace) with active membrane responses to a depolarizing (100 pA) current injection. *B*, ISO reduced tonic action potential firing frequency across all current pulses (5 cells, 3 animals; from 50 to 200 pA, two way RM ANOVA: interaction $F_{(6,24)} = 0.98$, $P = 0.460$, current injection $F_{(6,24)} = 27.55$, $P < 0.001$, ISO effect $F_{(1,4)} = 17.18$, $P = 0.014$). *C*, ISO reduced RMP (6 cells, 3 animals; paired two-tailed *t*-test: $t_{(5)} = 3.48$, $P = 0.018$) in WT mice. *D*, ISO did not change IR (paired two-tailed *t*-test: $t_{(5)} = 1.29$, $P = 0.252$) in WT mice. *E*, Original traces from a representative CeM WT neuron showing post-inhibitory rebound burst-firing before (black), after application of ISO (gray) and after wash (light gray trace). Burst-firing was induced by injection of a hyperpolarizing (–150 pA) current during 400 ms. *F*, Averaged LTS amplitude was reduced by the application of ISO across all hyperpolarizing current pulses from –25 to –225 pA in WT mice (7 cells, 3 animals; two-way RM ANOVA: interaction $F_{(8,48)} = 2.70$, $P = 0.015$, current injection $F_{(8,48)} = 20.56$, $P < 0.001$, ISO $F_{(1,6)} = 18.08$, $P = 0.005$, Sidak's post hoc presented in figure). *G*, Bar graph showing ISO significantly increased the threshold for the occurrence of LTS (6 cells, 3 animals; paired two-tailed *t*-test $t_{(5)} = 5.98$, $P = 0.002$). *H*, ISO had very little effect on average tonic firing frequency in $Ca_V3.1$ KO mice (6 cells, 3 animals; two way RM ANOVA: interaction $F_{(6,30)} = 8.07$, $P < 0.001$, current injection $F_{(6,30)} = 83.00$, $P < 0.001$, ISO effect $F_{(1,5)} = 4.36$, $P = 0.091$, Sidak's post hoc presented in figure). *I* and *J*, ISO did not affect RMP (paired two-tailed *t*-test: $t_{(5)} = 1.25$, $P = 0.268$) and IR (paired two-tailed *t*-test: $t_{(5)} = 1.46$, $P = 0.203$) in $Ca_V3.1$ KO mice. *$P < 0.05$, **$P < 0.01$, ***$P < 0.001$.

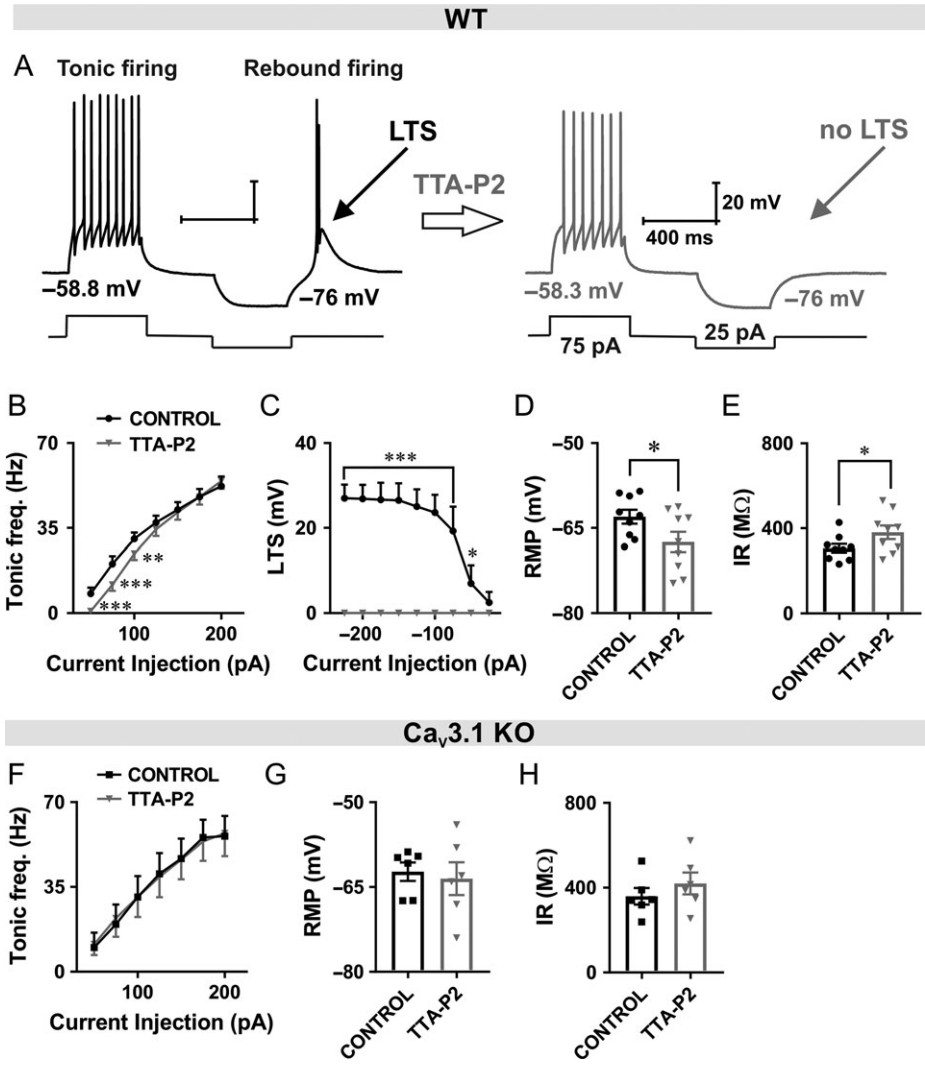


**Figure 6.** TTA-P2 reduced tonic and rebound burst firing in CeM neurons from WT mice. *A*, Original traces from a representative neuron after depolarizing (75 pA) and hyperpolarizing current injection (−25 pA) in the CeM before (left panel, black trace) and after application of TTA-P2 (right panel, gray trace). *B*, TTA-P2 reduced tonic action potential firing frequency across some current pulses (from 50 to 100 pA) in WT mice (9 cells, 4 animals; two way RM ANOVA: interaction $F_{(6,48)} = 5.68$, $P < 0.001$, current injection $F_{(6,48)} = 125.00$, $P < 0.001$, TTA-P2 $F_{(1,8)} = 2.79$, $P = 0.133$, Sidak's post hoc presented in figure). *C*, Graph of averaged traces of CeM neurons shows that LTS amplitude was completely abolished by the TTA-P2 application across all hyperpolarizing current pulses (9 cells, 4 animals; from −25 to −225 pA; two way RM ANOVA: interaction $F_{(8,64)} = 15.64$, $P < 0.001$, current injection $F_{(8,64)} = 15.64$, $P < 0.001$, TTA-P2 $F_{(1,8)} = 37.5$, $P < 0.001$, Sidak's post hoc presented in figure). *D* TTA-P2 decreased RMP (paired two-tailed *t*-test: $t_{(8)} = 3.11$, $P = 0.014$). *E*, TTA-P2 increased IR (paired two-tailed *t*-test: $t_{(8)} = 2.75$, $P = 0.025$) in WT mice. *F*, TTA-P2 did not have an effect on firing frequency recorded under the same recording condition in Ca$_V$3.1 KO mice (6 cells, 3 animals; two way RM ANOVA: interaction $F_{(6,30)} = 0.84$, $P = 0.550$, current injection $F_{(6,30)} = 47.51$, $P < 0.001$, TTA-P2 $F_{(1,5)} = 0.00$, $P = 0.989$). *G* and *H*, RMP (paired two-tailed *t*-test: $t_{(5)} = 0.64$, $P = 0.552$) and IR (paired two-tailed *t*-test: $t_{(5)} = 2.21$, $P = 0.078$) were not changed after TTA-P2 perfusion. *P < 0.05, **P < 0.01, ***P < 0.001.

frequency burst-firing pattern associated with thalamic LTS closely depends on T-current kinetics and that blockade of T-channels can alter neuronal excitability (Tscherter et al. 2011). Representative traces after depolarizing and hyperpolarizing current injection under baseline conditions in WT mice (black trace) and after TTA-P2 perfusion (gray trace) are presented in Figure 6A. Note that after application of TTA-P2, LTS was completely abolished. We also examined the effect of the TTA-P2 on the tonic-firing mode of CeM neurons in WT mice. We found that TTA-P2 reduced number of APs during tonic firing mode in WT mice similar to ISO (Fig. 6B).

Summary data during escalating current injections showed a complete abolition of LTS and rebound bursting after TTA-P2 application in WT animals (Fig. 6C). In addition, we found that TTA-P2 significantly hyperpolarized RMP and increased IR in WT mice (Fig. 6D,E, respectively).

In contrast, Figure 6F shows that TTA-P2 did not have any appreciative effect on tonic firing frequency recorded under the same recording condition in Ca$_V$3.1 KO mice. Moreover, TTA-P2 did not significantly affect RMP and IR in Ca$_V$3.1 KO mice (Fig. 6G,H, respectively). These data strongly suggest that inhibition of Ca$_V$3.1 T-currents underlies the effects of TTA-P2 on active and passive membrane properties of CeM neurons in WT mice. Hence, the use of complementary selective pharmacological probe and mouse genetics strongly suggest that most of the observed effects of ISO on excitability are mediated *via* inhibition of Ca$_V$3.1 channels in CeM neurons.

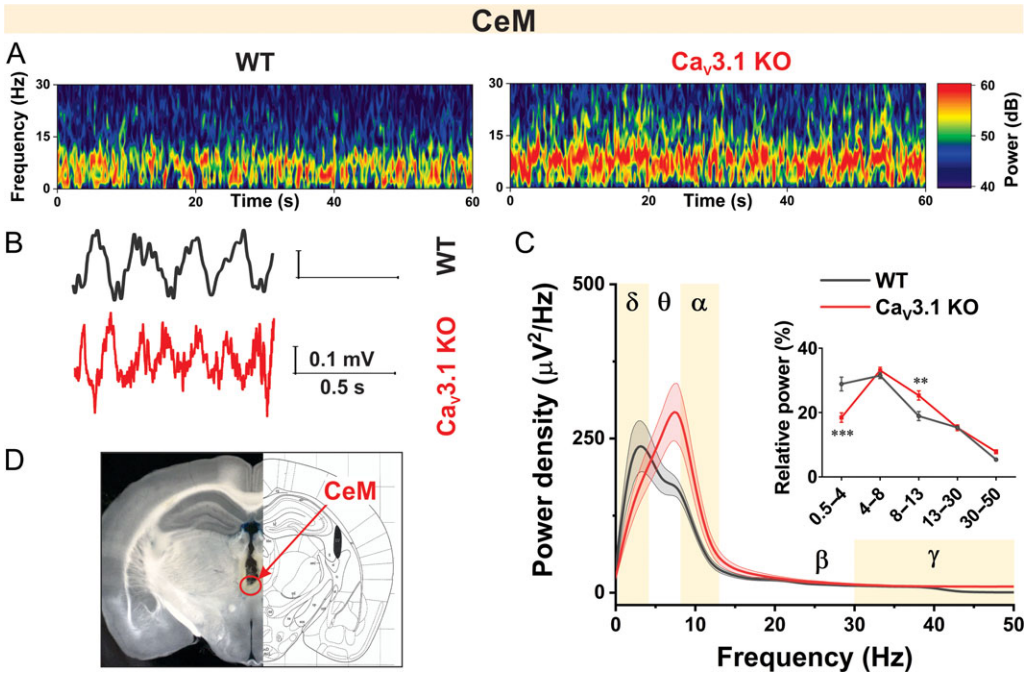


**Figure 7.** Oscillatory differences between WT and $Ca_V3.1$ KO mice in CeM during quiet awake state. *A*, Representative thalamic (CeM) spectrograms during quiet awake state from WT (left) and $Ca_V3.1$ KO (right) mice. *B*, Representative raw CeM traces from WT (gray) and $Ca_V3.1$ KO (red trace) mice. *C*, Power density and relative power (inset in figure) revealed decreased percentage of δ waves in $Ca_V3.1$ KO mice (two way RM ANOVA: interaction $F_{(4,60)} = 10.81$, $P < 0.001$, oscillations $F_{(4,60)} = 101.10$, $P < 0.001$, WT vs. mutant $F_{(1,15)} = 0.58$ $P = 0.458$, Sidak's post hoc presented in figure). *D*, Electrode placement conformation. WT – 7 animals, $Ca_V3.1$ KO – 10 animals; $^{**}P < 0.01$, $^{***}P < 0.001$.

## Oscillatory Differences Between WT and $Ca_V3.1$ KO Mice in CeM Recorded In Vivo

Based on the observed differences in AP firing patterns in our current-clamp experiments, we proposed that properties of thalamocortical oscillations in vivo might be different in CeM from WT and $Ca_V3.1$ KO mice. Thalamic cells generate rhythmic bursts of action potentials, resulting in 0.5–4 Hz oscillations (δ waves) and 7–14 Hz spindle activity during non-REM sleep (sleep spindles) (Yunker and McEnery 2003). Representative spectrograms from CeM during quiet awake behavior recorded from WT and $Ca_V3.1$ KO mice are presented in Figure 7*A*. Note that the observed frequency of LFPs recorded from WT mice was slower in comparison to $Ca_V3.1$ KO mice (original representative traces presented in Fig. 7*B*). Power density revealed peak density in WT mice in the δ frequency range, while the peak density was shifted towards the θ frequency range in $Ca_V3.1$ KO mice (Fig. 7*C*). Analysis of relative power (inset in Fig. 7*C*) revealed decreased percentage of δ and increased percentage of α oscillations in KO in comparison to WT mice. The correct electrode placement conformation is depicted in Figure 7*D*.

## Oscillatory Differences Between WT and $Ca_V3.1$ KO Mice in CeM During ISO-Induced Anesthesia

We next set out to test the hypothesis that $Ca_V3.1$ channels may play a significant role in the effects of ISO on the rhythmic oscillations of intact thalamocortical circuits, because in our in vitro current-clamp experiments we demonstrated that ISO strongly inhibited firing of APs and hyperpolarized CeM neurons in WT but not in $Ca_V3.1$ KO mice. Hence, we used LFP recordings in WT and $Ca_V3.1$ KO mice to investigate whether thalamic $Ca_V3.1$ channels are important for the slow oscillations in vivo during inhalational anesthesia with ISO. Representative spectrograms with original traces from CeM during administration of low anesthetic (1 vol%) and deep anesthetic concentrations (2 vol%) of ISO recorded from WT and $Ca_V3.1$ KO mice are presented in Figure 8*A*. We found that the $Ca_V3.1$ KO mice exhibited increased power in comparison to WT animals in all oscillations except in δ frequency range during administration of 1 vol% ISO. Power density under 1 vol% of ISO revealed peak density at 3.9 Hz in WT mice, and for $Ca_V3.1$ KO mice was shifted to around 5 Hz (Fig. 8*B*). Analysis of relative power (inset in Fig. 8*B*) revealed inability of 1 vol% of ISO to increase portion of δ oscillation in $Ca_V3.1$ KO mice (mean relative power about 24%), to the level seen in WT mice (mean relative power about 41%). Moreover, in contrast to decreased δ oscillations under ISO-induced anesthesia, we found that α and low γ oscillations were more dominant in $Ca_V3.1$ KO mice. Bottom traces and spectrograms in Figure 8*A* show that under deep anesthesia with 2 vol % ISO, a burst suppression-like pattern was observed in WT and mutant mice but with different oscillations distribution- with δ oscillations being more prominent during suppression phase in WT animals. During administration of 2 vol% of ISO peak in power density in WT mice was even more shifted towards slower oscillations (around 2 Hz), while in $Ca_V3.1$ KO mice shifted from 5 to 2 Hz (Fig. 8*C*). We also noted that under 2 vol% of ISO the power density was much lower in KO animals in comparison with WT mice (Fig. 8*C*). Additionally, we found that 2 vol % ISO increased the relative contribution of δ oscillation in $Ca_V3.1$ KO mice for about 32% and for about 41% in WT mice (inset in Fig. 8*C*).

In order to account for different baselines in δ frequency range between WT and mutant mice, the change of relative power (differences under anesthesia and baseline) was calculated. This parameter confirmed that in CeM during administration of 1 vol

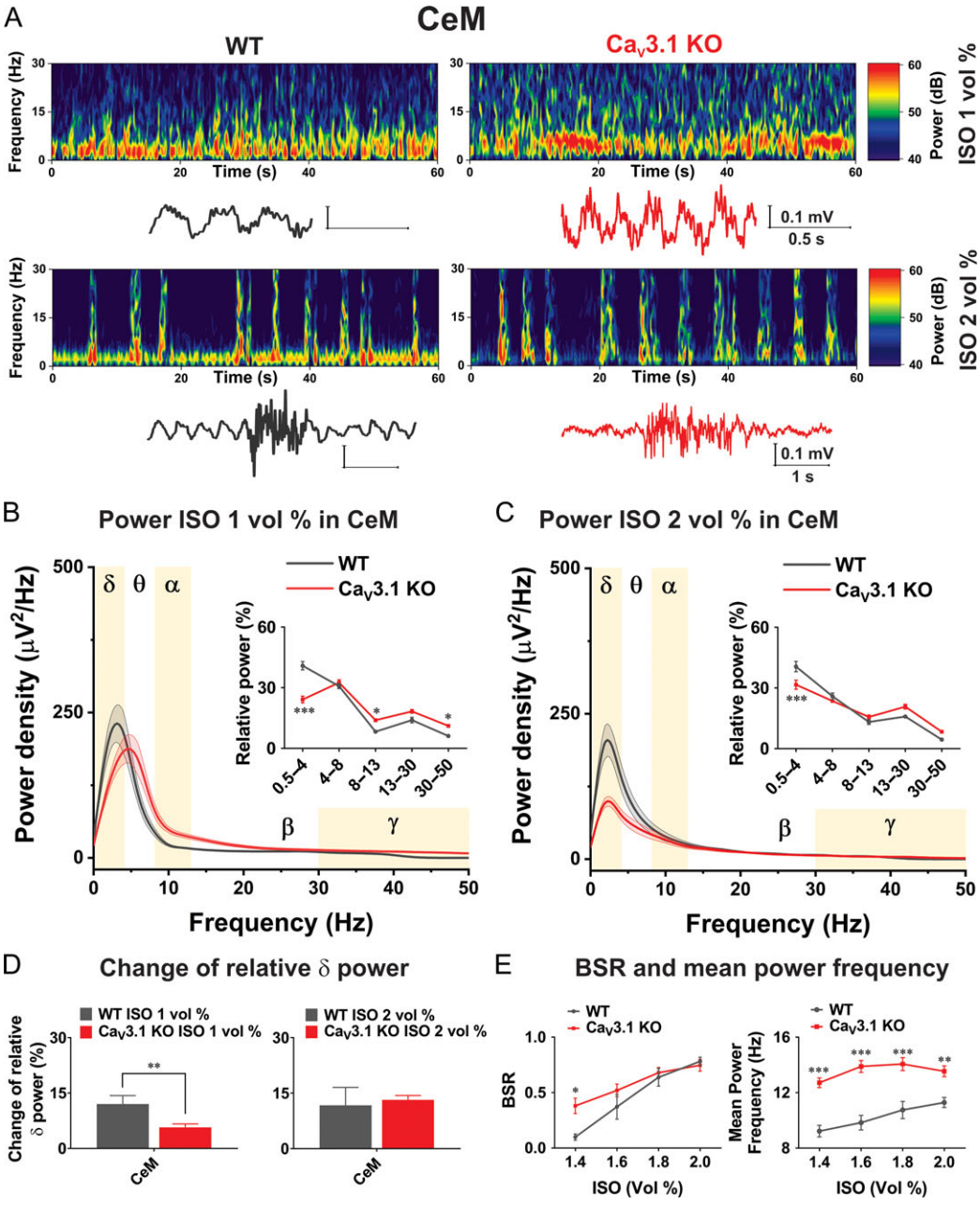


**Figure 8.** Oscillatory differences in CeM between WT and Ca$_V$3.1 KO mice during ISO anesthesia. *A*, Representative spectrograms with representative traces from CeM during 1 and 2 vol% of ISO anesthesia recorded from WT (left) and Ca$_V$3.1 KO (right) mice. *B*, Power density and relative power (inset in figure) revealed decreased percentage of δ and increased percentage in α and low γ waves in Ca$_V$3.1 KO mice under 1 vol% of ISO (two way RM ANOVA: $F_{(4,56)} = 22.24$, $P < 0.001$, oscillations $F_{(4,56)} = 128.20$, $P < 0.001$, WT vs. mutant $F_{(1,14)} = 0.10$, $P = 0.751$, Sidak's post hoc presented in figure). *C*, Power density and relative power (inset in figure) revealed inability of 2 vol% of ISO to increase percentage of δ waves in Ca$_V$3.1 KO mice to the level seen in WT mice (two way RM ANOVA: interaction $F_{(4,56)} = 6.25$, $P < 0.001$, oscillations $F_{(4,56)} = 95.65$, $P < 0.001$, WT vs. mutant $F_{(1,14)} = 1.11$, $P > 0.999$, Sidak's post hoc presented in figure). *D*, Change of relative δ power in CeM (relative power under ISO – relative power during baseline) revealed differences between WT and mutant mice in CeM under 1 vol% of ISO (unpaired two-tailed *t*-test: $t_{(14)} = 2.99$, $P = 0.010$). *E*, Suppression to burst ratio (BSR) revealed increased ratio in Ca$_V$3.1 KO mice under 1.4 vol% of ISO in compare to WT (two way RM ANOVA: interaction $F_{(3,42)} = 3.91$, $P = 0.015$, ISO vol% $F_{(3,42)} = 45.05$, $P < 0.001$, WT vs. mutant $F_{(1,14)} = 2.37$, $P = 0.146$, Sidak's post hoc presented in figure). Mean power frequency during non-suppression episodes revealed higher frequencies in Ca$_V$3.1 KO mice during ISO anesthesia (two way RM ANOVA: interaction $F_{(3,42)} = 3.76$, $P = 0.018$, ISO vol% $F_{(3,42)} = 12.32$, $P < 0.001$, WT vs. mutant $F_{(1,14)} = 34.29$, $P < 0.001$, Sidak's post hoc presented in figure) WT – 6 animals, Ca$_V$3.1 KO – 10 animals; $^*P < 0.05$, $^{**}P < 0.01$, $^{***}P < 0.001$.

% of ISO we found increased relative δ power for 12% in WT mice which was about 2-fold larger than increase seen in Ca$_V$3.1 KO mice of about 6% (Fig. 8*D*). In contrast, the change in relative δ power was not different between WT and mutant mice under 2 vol% of ISO anesthesia. In Figure 8*E* effect of ISO anesthesia on suppression-to-burst ratio (BSR) and mean power frequency during non-suppression episodes in CeM are shown. We found that BSR was about 4-fold higher during 1.4 vol% ISO administration in Ca$_V$3.1 KO than in WT mice, indicating greater suppression of thalamocortical information transfer in the mutant mice (left panel on Fig. 8*E*). Additionally, we found that mean power frequencies during non-suppression episodes were about 30%

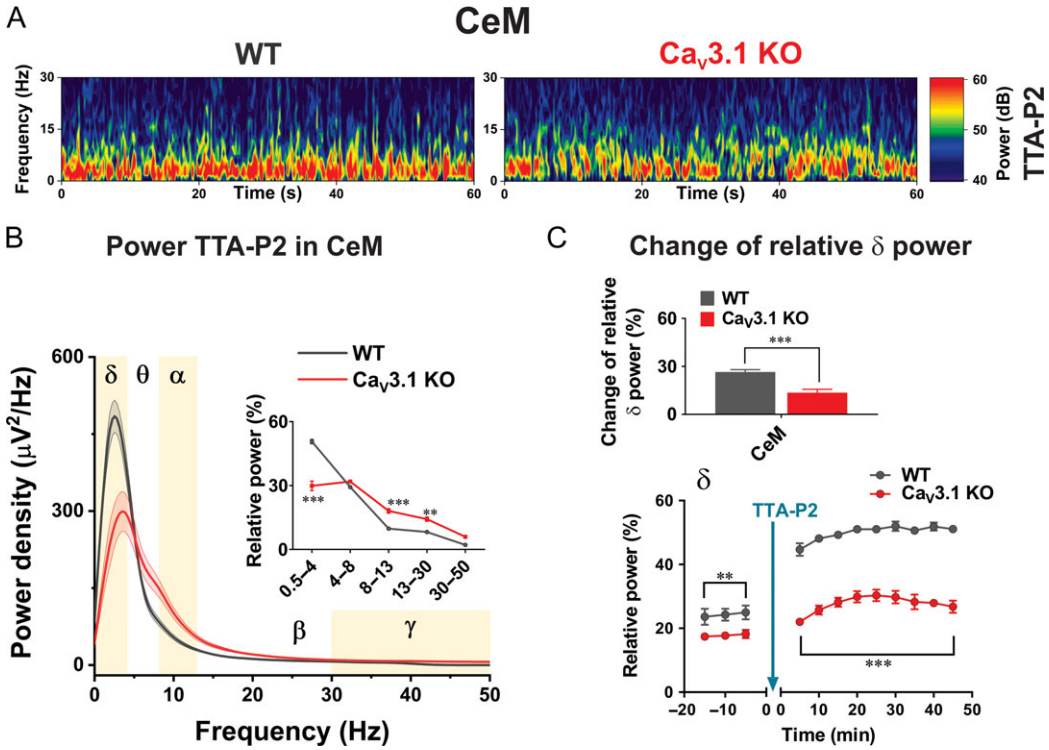


**Figure 9.** Oscillatory differences between WT and $Ca_V3.1$ KO mice in CeM during TTA-P2 administration in vivo. *A*, Representative spectrograms from CeM 30 min after i.p. injection of 60 mg/kg TTA-P2 recorded from WT (left) and $Ca_V3.1$ KO (right) mice. *B*, Power density and relative power (inset in figure) revealed decreased percentage of δ and increased percentage in α and β waves in $Ca_V3.1$ KO mice after TTA-P2 (two way RM ANOVA: $F_{(4,60)} = 43.87$, $P < 0.001$, oscillations $F_{(4,60)} = 279.50$, $P < 0.001$, WT vs. mutant $F_{(1,15)} = 1.31$, $P = 0.310$, Sidak's post hoc presented in figure). *C*, Change of relative δ power in CeM (relative power under TTA-P2 – relative power during baseline) revealed differences between WT and mutant mice (unpaired two-tailed *t*-test: $t_{(15)} = 4.57$, $P < 0.001$). Relative δ power across time during baseline revealed higher δ oscillations in WT animals (two way RM ANOVA: interaction $F_{(2,28)} = 0.09$, $P = 0.914$, time $F_{(2,28)} = 1.13$, $P = 0.336$, WT vs. mutant $F_{(1,14)} = 8.93$, $P < 0.01$). Additionally, there was higher relative δ power after TTA-P2 administration in WT mice during all recorded period (two way RM ANOVA: interaction $F_{(8112)} = 0.80$, $P = 0.604$, time $F_{(8112)} = 11.82$, $P < 0.001$, WT vs. mutant $F_{(1,14)} = 154.90$, $P < 0.001$). WT – 7 animals, $Ca_V3.1$ KO – 9–10 animals; $^*P < 0.05$, $^{**}P < 0.01$, $^{***}P < 0.001$.

higher in $Ca_V3.1$ KO mice under all ISO concentrations (right panel on Fig. 8*E*).

### Oscillatory Differences Between WT and $Ca_V3.1$ KO Mice in CeM During Systemic Administration of TTA-P2 In Vivo

The effects of selective pharmacological inhibitors of T-channels in vivo on arousal and sleep-generated δ waves were previously studied in thalamic circuitry. For example, administration of a another highly selective, potent T-channel inhibitor TTA-A2, given at 10 mg/kg orally for 5 days, resulted in decreased awake states and increased non-REM (δ) sleep in WT mice, but not in dual $Ca_V3.1$-$Ca_V3.3$ KO mice (Kraus et al. 2010). In another study, authors used direct local applications of TTA-P2 onto VB neurons with microdialysis, as well as systemic administration with i.p. injections during sleep, to demonstrate that TTA-P2 promoted slow frequency LFP waves (David et al. 2013). Although these studies strongly suggest that pharmacological antagonism of T-channels in vivo alters thalamocortical dynamics that underlie arousal, very little is known about properties of rhythmic oscillations of CeM neurons in vivo during systemic administration of selective T-channel inhibitors. Hence, we examined properties of rhythmic oscillations of CeM neurons in vivo after i.p. administration of TTA-P2. We chose a dose of 60 mg/kg of TTA-P2 that produced behavior consistent with sedation (decrease of movement and blunted response to stimulation, but not loss of righting reflex) in injected mice. Representative spectrograms from CeM at 30 min after i.p. application of 60 mg/kg TTA-P2 recorded from WT and $Ca_V3.1$ KO mice were presented in Figure 9*A*. Power density revealed a higher peak density of about 40% in the δ range in WT mice in comparison to $Ca_V3.1$ KO mice (Fig. 9*B*). Analysis of relative power (inset in Fig. 9*B*) revealed TTA-P2's inability to increase the portion of δ oscillation in $Ca_V3.1$ KO mice (mean relative power about 30%), to the level seen in WT mice (mean relative power of about 51%). In contrast to decreased δ oscillations, we found that α and β oscillations were more dominant in $Ca_V3.1$ KO mice when compared with WT mice after administration of TTA-P2. Importantly, when we considered baseline before drug administration, TTA-P2 increased relative δ power in CeM for about 26% in WT mice, which was about 2-fold higher than increase in $Ca_V3.1$ KO mice (top panel in Fig. 9*C*). On the bottom panel on Figure 9*C* effect of TTA-P2 on relative δ power in CeM across time is depicted. Note that the baseline recorded before injection of TTA-P2 confirmed the existence of higher δ frequency in WT in comparison to $Ca_V3.1$ KO mice. Moreover, the injection of TTA-P2 caused consistently about 2-fold greater increase in the relative δ power in WT animals when compared with the mutant mice up to 45 min of recording.

## Discussion

The thalamus is the major gateway of the flow of sensory information from the periphery to the cortex and the disruption of thalamocortical connectivity may be an essential common

feature of the hypnotic effects of many general anesthetics. Although the role of thalamic T-channels in natural sleep is reasonably well established, the role of these channels in anesthesia remains poorly understood. As a part of intralaminar complex of the thalamus, CeM is one of the non-specific nuclei of the limbic thalamus (Vertes et al. 2015; Gent et al. 2018). Recent studies revealed importance of CeM during induction of general anesthesia and transition into sleep (Baker et al. 2014; Gent et al. 2018). Furthermore, CeM is recognized as the neuroanatomic site mediating arousal response since microinfusion of the nicotine or voltage-gated potassium channel blockers into CeM could restore consciousness in the rats during administration of anesthetic agents (Alkire et al. 2007, 2009; Lioudyno et al. 2013). Here, we revealed for the first time that $Ca_V3.1$ isoform of T-channels plays an important role in regulation of excitability and rhythmic activity of CeM during ISO-induced anesthesia.

### $Ca_V3.1$ Channels in CeM Neurons are Important for Inhibitory Effects of ISO on Neuronal Excitability

Although molecular targets for general anesthetics are thought to be mainly ligand-gated ion channels such as gamma-aminobutyric acid type A ($GABA_A$) and *N*-methyl-D-aspartate (NMDA) receptors, there is evidence that some voltage-gated ion channels play a role in the sedative/hypnotic effects of anesthetics (Franks 2008; Orestes and Todorovic 2010). It has been shown that ISO blocks T-channels in VB and TRN neurons at clinically relevant concentrations (Ries and Puil 1999; Joksovic and Todorovic 2010; Eckle et al. 2012). Our voltage-clamp experiments demonstrated that ISO reduced T-current density, induced a hyperpolarizing shift in steady-state inactivation and decreased inactivation kinetics in CeM neurons. We then used ensuing current-clamp recordings to show that ISO hyperpolarized CeM neurons and inhibited both tonic and rebound burst firing in WT animals, these effects were not noted in $Ca_V3.1$ KO mice. Furthermore, pan-selective blocker of T-channels TTA-P2 also induced hyperpolarization, and inhibited tonic and rebound burst firing in WT but not in $Ca_V3.1$ null mice. Similarly to previous studies in VB thalamic neurons (Kim et al. 2001), our findings reveal the absence of rebound burst with LTS in CeM neurons without apparent changes in tonic firing in $Ca_V3.1$ KO mice.

Our voltage-clamp recordings demonstrated presence of characteristic T-currents in WT mice, which were lacking in $Ca_V3.1$ KO mice. In contrast, in experiments with TTA-P2, as we already described in rats (Stamenic and Todorovic 2018), pharmacological blockade of T-channels in CeM decreased tonic firing and produced loss of LTS firing in WT mice. However, we found that TTA-P2 did not alter tonic firing frequency in $Ca_V3.1$ KO mice. This is in accordance with previous reports that activation of T-channels in VB thalamic neurons plays a crucial role in tonic firing and regulates the sensory transfer during wakefulness (Tscherter et al. 2011; Deleuze et al. 2012). However, the lack of difference in the baseline tonic firing frequency between WT and $Ca_V3.1$ KO mice in our study and the study by Kim and colleagues (2001), strongly suggest that compensatory changes of other ionic currents in $Ca_V3.1$ KO mice may have occurred. This may also account for some of the differences between the present results and our previous work with rats (Stamenic and Todorovic 2018). This notion is supported by our voltage-clamp experiments that revealed the existence of HVA-like inward currents in $Ca_V3.1$ KO mice that are partially inhibited by SNX-482.

It is important to mention that in the study of Ries and Puil (1999), ISO-induced hyperpolarization of VB thalamic neurons was attributed to the increased background potassium conductance. However, our data in CeM neurons point to different mechanisms that depend critically on T-channels, because this effect is not seen in $Ca_V3.1$ KO mice. To this end, TTA-P2 likewise hyperpolarized CeM neurons from WT mice but not from $Ca_V3.1$ KO mice. We propose that this is likely due to inhibitory effect of ISO and TTA-P2 on T-type "window current" in CeM neurons (Fig. 1) which is also demonstrated in other thalamic neurons (Dreyfus et al. 2010; Eckle et al. 2012).

### $Ca_V3.1$ Channels in CeM Neurons are Important Contributors to the Slow Thalamocortical Oscillations During ISO-Induced Anesthesia

It is well established that neuronal T-channels play a crucial role in generation of thalamic δ oscillations as a dominant brain activity during sleep. Consistent with the differences in excitability in vitro, we also described different effects on intact thalamocortical circuits in vivo seen with ISO in WT mice and $Ca_V3.1$ null mice, which supports the existence of qualitative differences in ISO-induced anesthesia between WT and mutant mice. Under different behavioral states, the thalamus can generate not only spindle oscillations (7–14 Hz), but produces a slower δ rhythm consisting of LTS followed by afterhyperpolarizing potentials (Nuñez et al. 1992). Previously it has been speculated that the production of thalamic δ oscillations involves two intrinsic currents such as hyperpolarization-activated ($I_h$) current and T-current, at a hyperpolarized membrane potential (Nuñez et al. 1992). However, recent studies revealed that T-currents are sufficient to generate low threshold oscillations in δ band, while $I_h$ currents amplifies and stabilizes the oscillations (Amarillo et al. 2015). It has been shown that at the RMP of −60 mV thalamocortical neurons can generate spindle-like oscillations, whereas at more negative RMP (<−65 mV) neurons can trigger an oscillations within the δ frequency range (Steriade et al. 1991). Similarly, during thalamic hyperpolarization induced by blockade of NMDA receptors the most dominant frequency was in δ frequency range of about 3.5–4 Hz (Buzsáki 1991). Therefore, we infer that in our experiments hyperpolarization induced by ISO and TTA-P2 can contribute to increased δ frequency oscillations observed in our in vivo studies with WT mice. Conversely, diminished δ oscillation rise in $Ca_V3.1$ KO animals upon administration of TTA-P2 and ISO is likely related to the fact that TTA-P2 and ISO did not hyperpolarize CeM neurons in $Ca_V3.1$ null mice.

Previous studies have revealed several oscillations arising during sleep: a slow (<1 Hz) cortically generated, a clock-like thalamic δ oscillations (1–4 Hz), and cortical δ oscillations (1–4 Hz) (Amzica and Steriade 1998). Experiments with decorticated cats demonstrated that slow oscillations (<1 Hz) have cortical origin and that the pattern of δ oscillations (0.5–4 Hz) is shaped by the corticothalamic feedback (Timofeev and Steriade 1996). It is well established that loss of consciousness under ISO, sevoflurane and propofol anesthesia is associated with increase in δ oscillations in different species including humans (Flores et al. 2017; Guidera et al. 2017; Silva et al. 2018).

Our results are consistent with a recent study that revealed that low-frequency oscillations (especially in δ range) and that duration of hypnosis in $Ca_V3.1$ KO mice were decreased during sedation/hypnosis induced with ketamine and ethanol (Choi et al. 2015). This was a somewhat surprising finding given that ketamine and ethanol do not affect $Ca_V3.1$ T-current amplitudes

in vitro at clinically relevant concentrations (Todorovic et al. 2000; Shan et al. 2013). The authors proposed that this could be result of inhibition of NMDA currents and resulting hyperpolarization, which could deinactivate $Ca_V3.1$ channels. In contrast, Petrenko and colleagues (2007) reported that duration of ketamine-induced hypnosis was not different between WT and $Ca_V3.1$ KO mice. We propose that thalamic $Ca_V3.1$ channels may be directly or indirectly targeted by distinct classes of sedatives/hypnotics.

Although the blockade of T-channels could be in contradiction with the existence of δ and other slow oscillations, it has been shown that a partial T-channel block (as achieved here with ISO) could favor the presence of δ oscillations (David et al. 2016). Similarly, partial block of T-currents in thalamus and hyperpolarization due to inhibition of T-type "window current" achieved with i.p. administration of TTA-P2 could produce rise in δ oscillation and induce sedative effect in mice. Towards this end, it has been demonstrated that in vivo T-type channel inhibition by TTA-A2, an analog of TTA-P2, suppresses active wake and promotes slow-wave δ sleep in WT mice but not in mice lacking both $Ca_V3.1$ and $Ca_V3.3$ channels, suggesting the T-channel-specific effect of TTA-A2 on thalamocortical network activity (Kraus et al. 2010). These findings are supported by results that stable δ oscillations can be evoked with minimal T-type conductance (David et al. 2016). In contrast, it has been reasonably well established that pharmacological inhibition of thalamic T-type "window current" under urethane anesthesia in rats decreased slow δ oscillation in the <1 Hz frequency range (David et al. 2016).

## Compensatory Homeostatic Changes in Mice Lacking VGCCs and Thalamocortical Oscillations

It is well established that T-type channels and other isoforms of voltage-gated calcium channels (VGCCs) play a crucial role in regulation of neuronal excitability in sleep pathway. Hence, it is important to consider the influence of reported homeostatic compensatory changes that occurred in the mice lacking different subtypes of VGCCs. In our study we noticed a large shift of about 20 mV in activation kinetics between T-type currents recorded from WT animals and inward currents in $Ca_V3.1$ KO mice. Similar shift in activation kinetics (about 25 mV) and consequent lack of "window" current was reported for R-type calcium currents when compared with the T-currents (Randall and Tsien 1997; Nakashima et al. 1998). Based on different current kinetics and characteristic crisscross patterns of macroscopic T-current waveforms that were not described for R-type currents (Randall and Tsien 1997; Nakashima et al. 1998), we hypothesized that inward current seen in mutant mice could be a variant of R-type HVA currents. However, when we applied a relatively selective blocker of $Ca_V2.3$ R-type calcium channel SNX-482 (Newcomb et al. 1998), it inhibited inward currents from the mutant mice only partially. Towards this end, SNX-482-resistant variants of native R-type HVA currents have been reported previously (Newcomb et al. 1998, 2000). Hence, the partial inhibition that we observed in our experiment in $Ca_V3.1$ KO mice could be due to existence of SNX-482-resistant R-type calcium currents, and/or presence of other subtypes of HVA calcium currents.

In addition to low threshold (T-type mediated) calcium conductance responsible for slow oscillation, thalamocortical neurons can generate high-frequency oscillations by activating dendritic P/Q calcium channels (Pedroarena and Llinás 1997). Moreover, there is evidence that the genetic deletion of P/Q-type calcium channels generate larger compensatory T-currents and that there is an absence of subthreshold γ oscillations in $Ca_V2.1$ KO (P/Q calcium channels) mice (Zhang et al. 2002; Song et al. 2004; Llinás et al. 2007). Additionally, γ-band oscillations (centered to 40 Hz) formation is supported by resonance between thalamic and cortical structures, which confirmed the hypothesis that cognitive events depend on thalamocortical activity (Llinas et al. 1998).

On the other hand, besides voltage-dependent persistent sodium conductance, which plays a role in the genesis of the 10-Hz α oscillation, high threshold bursting (which occurs in a specialized subset of thalamocortical neurons) is responsible for the generation of locally synchronized α activity (Hughes and Crunelli 2005, 2007; Llinás 2014). Interestingly, repetitive high threshold bursting in thalamocortical cells occurs in 2–13 Hz, with higher frequency with stronger depolarization, the same component that underlie thalamic α oscillations can lead to θ rhythms when neurons are less depolarized (Hughes and Crunelli 2005). With that in mind, during α waves of relaxed state, action potential bursts in thalamocortical cells are driven by high threshold calcium spikes, that involve both T-channels and HVA L-type VGCCs (for review see Crunelli et al., 2018). In our experiments during relaxed awake state $Ca_V3.1$ null mice had less δ but more α oscillations in CeM, likely because of compensatory upregulation of HVA calcium currents. Similarly, during administration of lower concentrations of ISO in our in vivo study dominant oscillation in WT mice was δ rhythm, in comparison to $Ca_V3.1$ KO mice with prevailing θ oscillations. The noticed differences between WT and mutant mice during inhalation of 1 vol% of ISO in relative power such as larger α and γ band in $Ca_V3.1$ KO mice could again be the product of compensatory upregulation of HVA calcium currents. Similar to our study with ISO, during ketamine/ethanol induced hypnosis the low frequency δ rhythms were attenuated while the high frequency (α, β and γ) oscillations were increased in the $Ca_V3.1$ null mice (Choi et al. 2015).

Earlier studies showed that $Ca_V3.1$ KO mice had decreased thalamic δ oscillations and reduction in spindles during urethane and barbiturate-induced hypnosis (Lee et al. 2004, 2013). Likewise, during non-rapid eye movement (NREM) sleep, cortical power densities in the low frequencies including δ band (0.1–3 Hz) were decreased in $Ca_V3.1$ KO mice (Lee et al. 2004). On the contrary, there is evidence that during NREM sleep cortical spindles were not altered in $Ca_V3.1$ KO mice (Lee et al. 2013). Although, in this study we did not filter LFP recordings in a way that would allow analysis of the spindle component, we found that in CeM there is increased power density in mice lacking $Ca_V3.1$ channel during quiet awake state and under 1 vol% of ISO in spindle-like frequency range (8–13 Hz), but not under 2 vol% of ISO anesthesia. The reason for the discrepancies in all the mentioned studies is not known, but it is possible that region-specific compensation occurs in thalamocortical circuits in $Ca_V3.1$ KO mice.

## The Role of $Ca_V3.1$ Channels in ISO-Induced Burst Suppression Pattern of Intact Thalamocortical Circuits

Burst suppression is a characteristic LFP pattern with suppression phase – silenced cortical activity and burst phase – episodic high amplitude oscillations. While the precise neurophysiological mechanisms of burst-suppression patterns are not fully understood, it has been shown that burst-suppression has a cortical origin and that functional or anatomical impairment of cortical afferents leads to the burst-suppression pattern (Lukatch et al. 2005; Kroeger and Amzica 2007). It is well established that most clinically used anesthetics and some metabolic

abnormalities (e.g., profound acidosis, hypercapnia) can induce burst suppression LFP pattern. During burst suppression, cortical neurons become depolarized during burst episodes and hyperpolarized during silent periods, while some thalamic neurons may exhibit δ rhythm during silent-hyperpolarized states (Steriade et al. 1994). Our LFP recordings in vivo provide evidence that during inhalation of 2 vol% ISO, CeM neurons indeed generate δ oscillations during suppression mode in the WT mice, but not in the $Ca_V3.1$ KO mice. Importantly, the suppression to burst ratio (BSR) was about 4-fold higher during 1.4 vol% of ISO administration in $Ca_V3.1$ KO mice than in WT mice, indicating greater suppression of thalamocortical information transfer in the mutants. In our previous study we implicated $Ca_V2.3$ R-type HVA channels in suppression episodes during ISO-induced anesthesia (Joksovic et al. 2009; Joksovic and Todorovic 2010). However, the current study is to our knowledge the first evidence that establishes the importance of T-channels in contributing to this thalamic rhythmic activity during the silent period of burst suppression.

### Conclusions

Our results demonstrate, for the first time, the importance of thalamic $Ca_V3.1$ T-channels in thalamocortical oscillations from the non-specific thalamic nuclei that underlie clinically important effects of ISO. Further studies using selective pharmacology and mouse genetics in vivo are needed to determine relative contributions of other T-channel isoforms such as $Ca_V3.2$ and $Ca_V3.3$ that are prominent in different thalamic nuclei, and are also inhibited with clinically relevant concentrations of volatile anesthetics including ISO.

## Funding

This study was funded in part by grants from the National Institutes of Health (GRANT# R01GM102525 to S.M.T.).

## Notes

We thank Dr Nathalie Leresche on critical evaluation of our manuscript. *Conflict of Interest*: The authors received no compensation nor do they have any conflicting financial interests in regards to the work described in this manuscript.

## References

Accorsi A, Valenti S, Barbieri A, Raffi GB, Violante FS. 2003. Enflurane as an internal standard in monitoring halogenated volatile anaesthetics by headspace gas chromatography-mass spectrometry. J Chromatogr A. 985:259–264.

Alkire MT, Asher CD, Franciscus AM, Hahn EL. 2009. Thalamic microinfusion of antibody to a voltage-gated potassium channel restores consciousness during anesthesia. Anesthesiology. 110:766–773.

Alkire MT, McReynolds JR, Hahn EL, Trivedi AN. 2007. Thalamic microinjection of nicotine reverses sevoflurane-induced loss of righting reflex in the rat. Anesthesiology. 107:264–272.

Amarillo Y, Mato G, Nadal MS. 2015. Analysis of the role of the low threshold currents IT and Ih in intrinsic delta oscillations of thalamocortical neurons. Front Comput Neurosci. 9:1–9.

Amzica F, Steriade M. 1998. Electrophysiological correlates of sleep delta waves. Electroencephalogr Clin Neurophysiol. 107:69–83.

Baker R, Gent TC, Yang Q, Parker S, Vyssotski A, Wisden W, Brickley SG, Franks NP. 2014. Altered activity in the central medial thalamus precedes changes in the neocortex during transitions into both sleep and propofol anesthesia. J Neurosci. 34:13326–13335.

Buzsáki G. 1991. The thalamic clock: emergent network properties. Neuroscience. 41:351–364.

Chen Y, Parker WD, Wang K. 2014. The role of T-type calcium channel genes in absence seizures. Front Neurol. 5:1–8.

Cheong E, Shin HS. 2013. T-type Ca2+ channels in normal and abnormal brain functions. Physiol Rev. 93:961–992.

Choe W, Messinger RB, Leach E, Eckle VS, Obradovic A, Salajegheh R, Jevtovic-Todorovic V, Todorovic SM. 2011. TTA-P2 is a potent and selective blocker of T-type calcium channels in rat sensory neurons and a novel antinociceptive agent. Mol Pharmacol. 80:900–910.

Choi S, Yu E, Lee S, Llinás RR. 2015. Altered thalamocortical rhythmicity and connectivity in mice lacking CaV3.1 T-type Ca 2+ channels in unconsciousness. Proc Natl Acad Sci USA. 112:7839–7844.

Crunelli V, Lőrincz ML, Connelly WM, David F, Hughes SW, Lambert RC, Leresche N, Errington AC. 2018. Dual function of thalamic low-vigilance state oscillations: rhythm-regulation and plasticity. Nat Rev Neurosci. 19:107–118.

David F, Crunelli V, Leresche N, Lambert RC. 2016. Dynamic analysis of the conditional oscillator underlying slow waves in thalamocortical neurons. Front Neural Circuits. 10:1–11.

David F, Schmiedt JT, Taylor HL, Orban G, Di Giovanni G, Uebele VN, Renger JJ, Lambert RC, Leresche N, Crunelli V. 2013. Essential thalamic contribution to slow waves of natural sleep. J Neurosci. 33:19599–19610.

Deleuze C, David F, Béhuret S, Sadoc G, Shin HS, Uebele VN, Renger JJ, Lambert RC, Leresche N, Bal T. 2012. T-type calcium channels consolidate tonic action potential output of thalamic neurons to neocortex. J Neurosci. 32:12228–12236.

DiGruccio MR, Joksimovic S, Joksovic PM, Lunardi N, Salajegheh R, Jevtovic-Todorovic V, Beenhakker MP, Goodkin HP, Todorovic SM. 2015. Hyperexcitability of rat thalamocortical networks after exposure to general anesthesia during brain development. J Neurosci. 35:1481–1492.

Dreyfus FM, Tscherter A, Errington AC, Renger JJ, Shin H-S, Uebele VN, Crunelli V, Lambert RC, Leresche N. 2010. Selective T-type calcium channel block in thalamic neurons reveals channel redundancy and physiological impact of ITwindow. J Neurosci. 30:99–109.

Eckle VS, DiGruccio MR, Uebele VN, Renger JJ, Todorovic SM. 2012. Inhibition of T-type calcium current in rat thalamocortical neurons by isoflurane. Neuropharmacology. 63:266–273.

Flores FJ, Hartnack KE, Fath AB, Kim S-E, Wilson MA, Brown EN, Purdon PL. 2017. Thalamocortical synchronization during induction and emergence from propofol-induced unconsciousness. Proc Natl Acad Sci USA. 114:6660–6668.

Franks NP. 2008. General anaesthesia: from molecular targets to neuronal pathways of sleep and arousal. Nat Rev Neurosci. 9:370–386.

Franks NP, Lieb WR. 1993. Selective action of volatile general anaesthetics at molecular and cellular levels. Br J Anaesth. 71:65–76.

Gent TC, Bandarabadi M, Herrera CG, Adamantidis AR. 2018. Thalamic dual control of sleep and wakefulness. Nat Neurosci. 21:974–984.

Guidera JA, Taylor NE, Lee JT, Vlasov KY, Pei J, Stephen EP, Mayo JP, Brown EN, Solt K. 2017. Sevoflurane induces

coherent slow-delta oscillations in rats. Front Neural Circuits. 11:1–13.

Huc S, Monteil A, Bidaud I, Barbara G, Chemin J, Lory P. 2009. Regulation of T-type calcium channels: signalling pathways and functional implications. Biochim Biophys Acta. 1793: 947–952.

Hughes SW, Crunelli V. 2005. Thalamic mechanisms of EEG alpha rhythms and their pathological implications. Neuroscientist. 11:357–372.

Hughes SW, Crunelli V. 2007. Just a phase they're going through: the complex interaction of intrinsic high-threshold bursting and gap junctions in the generation of thalamic α and θ rhythms. Int J Psychophysiol. 64:3–17.

Jhangiani-Jashanmal IT, Yamamoto R, Gungor Z, Paré D, Gungor NZ, Paré D. 2016. Electroresponsive properties of rat central medial thalamic neurons. J Neurophysiol. 115: 1533–1541.

Joksovic PM, Todorovic SM. 2010. Isoflurane modulates neuronal excitability of the nucleus reticularis thalami in vitro. Ann N Y Acad Sci. 1199:36–42.

Joksovic PM, Weiergraber M, Lee W, Struck H, Schneider T, Todorovic SM. 2009. Isoflurane-sensitive presynaptic R-Type calcium channels contribute to inhibitory synaptic transmission in the rat thalamus. J Neurosci. 29:1434–1445.

Jones EG. 2001. The thalamic matrix and thalamocortical synchrony. Trends Neurosci. 24:595–601.

Kim D, Song I, Keum S, Lee T, Jeong MJ, Kim SS, McEnery MW, Shin HS. 2001. Lack of the burst firing of thalamocortical relay neurons and resistance to absence seizures in mice lacking α1G T-type Ca2+ channels. Neuron. 31:35–45.

Kraus RL, Li Y, Gregan Y, Gotter AL, Uebele VN, Fox SV, Doran SM, Barrow JC, Yang ZQ, Reger TS, et al. 2010. In vitro characterization of T-type calcium channel antagonist TTA-A2 and in vivo effects on arousal in mice. J Pharmacol Exp Ther. 335:409–417.

Kroeger D, Amzica F. 2007. Hypersensitivity of the anesthesia-induced comatose brain. J Neurosci. 27:10597–10607.

Lee J, Kim D, Shin HS. 2004. Lack of delta waves and sleep disturbances during non-rapid eye movement sleep in mice lacking alpha1G-subunit of T-type calcium channels. Proc Natl Acad Sci USA. 101:18195–18199.

Lee J, Song K, Lee K, Hong J, Lee H, Chae S, Cheong E, Shin HS. 2013. Sleep spindles are generated in the absence of T-type calcium channel-mediated low-threshold burst firing of thalamocortical neurons. Proc Natl Acad Sci USA. 110: 20266–20271.

Leresche N, Lambert RC. 2017. T-type calcium channels in synaptic plasticity T-type calcium channels in synaptic plasticity. Channels. 11:121–139.

Lioudyno MI, Birch AM, Tanaka BS, Sokolov Y, Goldin AL, Chandy KG, Hall JE, Alkire MT. 2013. Shaker-related potassium channels in the central medial nucleus of the thalamus are important molecular targets for arousal suppression by volatile general anesthetics. J Neurosci. 33:16310–16322.

Llinas R, Ribary U, Contreras D, Pedroarena C. 1998. The neuronal basis for consciousness. Philos Trans R Soc Lond B Biol Sci. 353:1841–1849.

Llinás RR. 2014. Intrinsic electrical properties of mammalian neurons and CNS function: a historical perspective. Front Cell Neurosci. 8:1–14.

Llinás RR, Choi S, Urbano FJ, Shin HS. 2007. Gamma-band deficiency and abnormal thalamocortical activity in P/Q-type channel mutant mice. Proc Natl Acad Sci USA. 104: 17819–17824.

Lukatch HS, Kiddoo CE, MacIver MB. 2005. Anesthetic-induced burst suppression EEG activity requires glutamate-mediated excitatory synaptic transmission. Cereb Cortex. 15:1322–1331.

Mandal PK, Pettegrew JW. 2008. Clinically relevant concentration determination of inhaled anesthetics (halothane, isoflurane, sevoflurane, and desflurane) by 19F NMR. Cell Biochem Biophys. 52:31–35.

Miwa H, Kondo T. 2011. T-type calcium channel as a new therapeutic target for tremor. Cerebellum. 10:563–569.

Nakashima YM, Todorovic SM, Pereverzev A, Hescheler J, Schneider T, Lingle CJ. 1998. Properties of Ba2+ currents arising from human α1E and α1Eβ3 constructs expressed in HEK293 cells: physiology, pharmacology, and comparison to native T-type Ba2+ currents. Neuropharmacology. 37:957–972.

Newcomb R, Chen X, Dean R, Dayanithi G, Cong R, Szoke B, Lemos J, Bowersox S, Miljanich G. 2000. SNX-482: a novel class E calcium channel antagonist from tarantula venom. CNS Drug Rev. 6:153–173.

Newcomb R, Szoke B, Palma A, Wang G, Chen XH, Hopkins W, Cong R, Miller J, Urge L, Tarczy-Hornoch K, et al. 1998. Selective peptide antagonist of the class E calcium channel from the venom of the tarantula Hysterocrates gigas. Biochemistry. 37:15353–15362.

Nuñez A, CurróDossi R, Contreras D, Steriade M. 1992. Intracellular evidence for incompatibility between spindle and delta oscillations in thalamocortical neurons of cat. Neuroscience. 48:75–85.

Orestes P, Todorovic SM. 2010. Are neuronal voltage-gated calcium channels valid cellular targets for general anesthetics? Channels (Austin). 4:518–522.

Pedroarena C, Llinás R. 1997. Dendritic calcium conductances generate high-frequency oscillation in thalamocortical neurons. Proc Natl Acad Sci USA. 94:724–728.

Pereira de Vasconcelos A, Cassel JC. 2015. The nonspecific thalamus: a place in a wedding bed for making memories last? Neurosci Biobehav Rev. 54:175–196.

Perez-Reyes E. 2003. Molecular physiology of low-voltage-activated t-type calcium channels. Physiol Rev. 83:117–161.

Petrenko AB, Tsujita M, Kohno T, Sakimura K, Baba H. 2007. Mutation of 1G T-type calcium channels in mice does not change anesthetic requirements for loss of the righting reflex and minimum alveolar concentration but delays the onset of anesthetic induction. Anesthesiology. 106:1177–1185.

Randall AD, Tsien RW. 1997. Contrasting biophysical and pharmacological properties of T-type and R-type calcium channels. Neuropharmacology. 36:879–893.

Ries CR, Puil E. 1999. Mechanism of anesthesia revealed by shunting actions of isoflurane on thalamocortical neurons. J Neurophysiol. 81:1795–1801.

Saalmann YB. 2014. Intralaminar and medial thalamic influence on cortical synchrony, information transmission and cognition. Front Syst Neurosci. 8:1–8.

Shan HQ, Hammarback JA, Godwin DW. 2013. Ethanol inhibition of a T-type Ca2+ channel through activity of protein kinase C. Alcohol Clin Exp Res. 37:1333–1342.

Shipe WD, Barrow JC, Yang Z, Lindsley CW, Yang FV, Schlegel KS, Shu Y, Rittle KE, Bock MG, Hartman GD, et al. 2008. Design, synthesis, and evaluation of a novel 4-aminomethyl-4-fluoropiperidine as a T-Type Ca 2 + channel antagonist. J Med Chem. 51:3692–3695.

Silva A, Cardoso-Cruz H, Silva F, Galhardo V, Antunes L. 2018. Comparison of anesthetic depth indexes based on thalamocortical local field potentials in rats. Anesthesiology. 112: 355–363.

Simms BA, Zamponi GW. 2014. Neuronal voltage-gated calcium channels: structure, function, and dysfunction. Neuron. 82: 24–45.

Song I, Kim D, Choi S, Sun M, Kim Y, Shin HS. 2004. Role of the 1G T-type calcium channel in spontaneous absence seizures in mutant mice. J Neurosci. 24:5249–5257.

Sonner JM, Gong D, Li J, Eger EI, Laster MJ. 1999. Mouse strain modestly influences minimum alveolar anesthetic concentration and convulsivity of inhaled compounds. Anesth Analg. 89:1030–1034.

Sonner JM, Werner DF, Elsen FP, Xing Y, Liao M, Harris RA, Harrison NL, Fanselow MS, Eger EI, Homanics GE. 2007. Effect of isoflurane and other potent inhaled anesthetics on minimum alveolar concentration, learning, and the righting reflex in mice engineered to express α1 γ-aminobutyric acid type A receptors unresponsive to isoflurane. Anesthesiology. 106:107–113.

Stamenic TT, Todorovic SM. 2018. Cytosolic ATP relieves voltage-dependent inactivation of T-Type calcium channels and facilitates excitability of neurons in the rat central medial thalamus. eNeuro. 5:1–16.

Steriade M, Amzica F, Contreras D. 1994. Cortical and thalamic cellular correlates of electroencephalographic burst-suppression. Electroencephalogr Clin Neurophysiol. 90:1–16.

Steriade M, Dossi RC, Nuñez A. 1991. Network modulation of a slow intrinsic oscillation of cat thalamocortical neurons implicated in sleep delta waves: cortically induced synchronization and brainstem cholinergic suppression. J Neurosci. 11:3200–3217.

Talley EM, Cribbs LL, Lee JH, Daud A, Perez-Reyes E, Bayliss D. 1999. Differential distribution of three members of a gene family encoding low voltage-activated (T-type) calcium channels. J Neurosci. 19:1895–1911.

Timofeev I, Steriade M. 1996. Low-frequency rhythms in the thalamus of intact-cortex and decorticated cats. J Neurophysiol. 76:4152–4168.

Todorovic SM, Perez-Reyes E, Lingle CJ. 2000. Anticonvulsants but not general anesthetics have differential blocking effects on different T-type current variants. Mol Pharmacol. 58: 98–108.

Tscherter A, David F, Ivanova T, Deleuze C, Renger JJ, Uebele VN, Shin HS, Bal T, Leresche N, Lambert RC. 2011. Minimal alterations in T-type calcium channel gating markedly modify physiological firing dynamics. J Physiol. 589: 1707–1724.

Van Der Werf YD, Witter MP, Groenewegen HJ. 2002. The intralaminar and midline nuclei of the thalamus. Anatomical and functional evidence for participation in processes of arousal and awareness. Brain Res Rev. 39:107–140.

Vertes RP, Hoover WB, Rodriguez JJ. 2012. Projections of the central medial nucleus of the thalamus in the rat: Node in cortical, striatal and limbic forebrain circuitry. Neuroscience. 219:120–136.

Vertes RP, Linley SB, Hoover WB. 2015. Limbic circuitry of the midline thalamus. Neurosci Biobehav Rev. 54:89–107.

Yunker AMR, McEnery MW. 2003. Low-voltage-activated ("T-Type") calcium channels in review. J Bioenerg Biomembr. 35:533–575.

Zhang Y, Mori M, Burgess DL, Noebels JL. 2002. Mutations in high-voltage-activated calcium channel genes stimulate low-voltage-activated currents in mouse thalamic relay neurons. J Neurosci. 22:6362–6371.